FOURIER TRANSFORM ION CYCLOTRON RESONANCE MASS SPECTROMETRY
INVESTIGATION OF GAS-PHASE IONS

By

DAVID KAGE

A DISSERTATION PRESENTED TO THE GRADUATE SCHOOL
OF THE UNIVERSITY OF FLORIDA IN PARTIAL FULFILLMENT
OF THE REQUIREMENTS FOR THE DEGREE OF
DOCTOR OF PHILOSOPHY

UNIVERSITY OF FLORIDA

1999

This dissertation is dedicated to the memory of my grandmother, Lila M. Brown, who would have laughed at all of this gobbledegook.

ACKNOWLEDGMENTS

There are many individuals whom I would like to thank that have contributed to my educational experience. Firstly, I would like to thank all of the previous and present members of the group. It was by working side-by-side with them, that most of this work was accomplished. The knowledge shared by all and passed through the ranks was invaluable. A big thank you goes out to Dr. Clifford H. Watson for always being there to answer basic questions. His knowledge of electronics, instrumentation, and trouble-shooting was a very big plus to have in the laboratory. I would like to thank Professor John R. Eyler for having the patience to let me stick around and try my best.

My appreciation goes out to Professor Laszlo Prokai for the knowledge and assistance he gave me during the cyclodextrin project. Professor Martin Vala was very helpful on the polycyclic aromatic hydrocarbon project in more ways than one. Dr. Jan Szczepanski was extremely generous in helping me get the polycyclic aromatic hydrocarbon project off and going. His assistance with laser-oriented questions was always appreciated. I would like to thank the remaining members of my committee (Professors William Weltner, Robert Hanhrahan, and Lisa McElwee-White) for always having an open door if I needed to seek scientific advice or if I just wanted to discuss current events.

TABLE OF CONTENTS

LIST OF TABLES

xi

xiv

Abstract of Dissertation Presented to the Graduate
School of the University of Florida in Partial Fulfillment
of the Requirements for the Degree of Doctor of Philosophy

FOURIER TRANSFORM ION CYCLOTRON RESONANCE MASS SPECTROMETRY
INVESTIGATION OF GAS-PHASE IONS

By

David Kage

December 1999

Chairman: Dr. John R. Eyler
Major Department: Chemistry

Fourier transform ion cyclotron mass spectrometry (FT-ICR MS) has received

considerable attention for its ability to make mass measurements with a combination of

resolution and accuracy that is higher than any other mass spectrometer. It can be used to

obtain high-resolution mass spectra from ions generated by practically every known

ionization method, to perform tandem mass spectrometric measurements, and to examine ion

chemistry and photochemistry. Its versatility follows from the fact that it is an ion trapping

instrument. The instrument mass analyzes and detects ions using methods which are unique

among mass spectrometers.

FT-ICR MS was used to measure the binding energies of cyclodextrin:amino acid

complexes in the gas-phase. Cyclodextrins are cyclic oligosaccharides that form truncated,

cone-shaped molecules. The most common are referred to as α-, β-, and

γ-cyclodextrin, which contain 6, 7, and 8 glucose units in the ring, respectively. The cavity that is formed by these molecules is hydrophobic, which lends to their ability as a "host" molecule for the study of host-guest chemistry. Collision-induced dissociation was used to measure the binding energies between the cyclodextrin host molecules and amino acid guest ions.

FT-ICR MS was also used to study the photodissociation of polycyclic aromatic hydrocarbon cations that are of interstellar importance. It has become a widely accepted notion that PAH cations are the carriers of the diffuse interstellar bands that have been measured for years by astronomers. The unknown link is to find exactly what PAH cations are responsible for the bands. Experiments have been performed to answer this question. Two major themes are repeated for the fluorene, acenaphthylene, diphenylacetylene, and naphthalene cations: monitoring the generation of new ions formed as a function of trapping time in the analyzer cell, and analyzing the products that are generated after irradiation from a xenon arc lamp. Results from the first series of experiments reveal that new ions are being formed which result from ion-molecule reactions between neutral parents and parent ions. The second set of experiments show that the ions generated from the ion-molecule reactions are fragmenting into smaller ions as a result of the irradiation from the xenon arc lamp.

HISTORICAL INCEPTION AND FUNDAMENTAL PRINCIPLES
OF FOURIER TRANSFORM ION CYCLOTRON
RESONANCE MASS SPECTROMETRY

Introduction

Fourier transform ion cyclotron resonance mass spectrometry (FT-ICR MS) has,
in recent years, developed into a very powerful analytical technique after years of
promising anticipation. Since 1985, this technique has been the subject of four journal
special issues,[1-4] three books,[5-7] and more than 60 review articles.[8] As of 1998 there were
over 235 FT-ICR mass spectrometers located in several countries around the world that
are being used to solve problems by a wide variety of scientists from analytical and
physical chemists in academic settings to drug discovery scientists in the pharmaceutical
community. In a relatively short time, FT-ICR MS has established itself as a powerful
mass spectrometric technique that combines the advantages of ultra-high mass resolution
and mass accuracy, is capable of utilizing a wide variety of ionization techniques, and can
use a wide range of methods for structure characterization of the primary sample ions.
With future improvements in magnet technology and with cheaper and more powerful
computers, this technique will surely become the method of choice for mass spectrometry
in the future.

<u>Historical Overview</u>

Fourier transform ion cyclotron resonance mass spectrometry is a mass spectrometric technique, whose beginnings can be traced back to conventional ICR mass spectrometry and Fourier transform nuclear magnetic resonance (FT-NMR) spectroscopy. The fundamental principles underlying ICR mass spectrometry were explained in 1930 by Ernest O. Lawrence[9] who invented the cyclotron particle accelerator (he was later awarded the Nobel Prize in physics in 1939 for this development). In 1932 Lawrence first demonstrated that a charged particle moving perpendicular to a uniform magnetic field is constrained to a circular orbit.[10] An orbit in which the angular frequency of the particle's motion is independent of the particle's orbital radius is characterized by the so-called cyclotron equation

$$\omega = qB/m \tag{1}$$

where ω is the angular frequency, q is the charge on the particle, B is the magnetic field strength, and m is the mass of the particle. Lawrence demonstrated that the cyclotron motion of a particle could be excited to a larger orbital radius by applying a transverse alternating electric field whose frequency matched the cyclotron frequency of the particle. This was a very significant discovery in that he demonstrated that a particle could be excited to a very large kinetic energy by use of small electric fields. The cyclotron particle accelerator has been a tremendous research tool used in the field of nuclear physics.

The first use in an analytical sense of the mass selective characteristics of the cyclotron motion of ions was the development of the Omegatron at the National Bureau of Standards by Sommer *et al.* in 1949.[11-13] Their instrument used the frequency-selective cyclotron acceleration of ions by a radio frequency (RF) field, into an electrometer collector that detected the current produced by the ions that were ejected from a cell. Their instrument was designed to achieve the common objectives of early mass spectrometer development: high mass resolving power and high abundance sensitivity. They obtained the objectives, but due to stringent stability requirements for the electronics and for the need of a very high vacuum, the instrument was never commercially produced as a general purpose mass spectrometer. It did find service as an affordable analyzer for leak detection.

The modern-day instrument can trace its direct ancestry back to the ICR spectrometer that was constructed in the mid-1960s in a collaborative effort between John Baldeschwieler's laboratory at Stanford University and a group of scientists at Varian Associates led by Peter Llewellyn.[14] The ICR technique soon became widely recognized as a preferred tool in the novel field of gas-phase ion chemistry with several instruments installed for basic research. These early instruments did have their share of disadvantages, primarily slow scan speeds and low mass resolution. With these limitations, it is obvious why the 1970s did not see the advent of a commercially available instrument. Even so, the limited number of instruments opened up new areas for researchers; they provided an avenue to study ion-molecule chemistry, ion thermochemistry, and ion spectroscopy unavailable to them previously.

Possibly the most important period of evolution for the technique was initiated by professors Alan Marshall and Melvin Comisarow when they began to apply FT methods (which were universally accepted in the field of NMR spectroscopy) to the handling of ICR data. But before they could be successful, several key technological problems had to be mastered. The major setbacks included: 1) lack of a suitable means of storing a range of ions of widely varying mass-to-charge ratio (m/z) simultaneously for the length of time needed to perform a mass measurement by the FT method, 2) lack of a feasible method to allow resonant excitation of all ions over a broad m/z range (broadband excitation), 3) an acceptable method to detect all ions simultaneously, and 4) lack of a fast digitizer with sufficient memory and bit resolution available at that time. The full advantages of FT-ICR MS would not be appreciated until these major obstacles were overcome.

McIver solved the problem of ion storage with the development of the trapped ion cell in 1970.[15] Comisarow was able to solve the problem of broadband excitation by applying a rapid frequency sweep of a few tens of volts amplitude. This would be capable of exciting a wide mass range of ions, but in a much shorter time (as compared to a slow frequency sweep with an amplitude of a few millivolts used to excite one ion at a time over a long period). To detect all the ions simultaneously, Marshall and Comisarow decided to measure the image current induced in a set of nearby electrodes by the packet of ions undergoing cyclotron motion. With most of the technological obstacles solved, Marshall and Comisarow demonstrated the advantages of the FT mode of operation of ICR mass spectrometry in 1973.[16-18] The advantages of speed, high resolution, and effective computer data processing that accompanied the advent of FT techniques made

the instrument much more attractive as an analytical MS tool. After a few developmental years, Nicolet Instruments (now Finnigan) manufactured a commercial FT-ICR mass spectrometer in 1981. Today, three companies market and sell FT-ICR mass spectrometers with the number of instruments used for studying the chemistry of gas-phase ions rising to over 235.

The Basic Apparatus

An FT-ICR instrument is a mass spectrometer, in other words, an instrument that observes the abundance of ions, resolved according to their masses. Most mass spectrometers operate on the basis of spatially separating the ions through a mass-dependent feature of their motion in a series of magnetic and/or electric fields while collecting the ions of different masses separately onto a detector. The FT-ICR approach is quite different since the ions are observed without separation or collection. The method is facilitated by using the absorption and emission of RF energy at the ion's characteristic (mass-dependent) cyclotron frequency as the ion undergoes cyclotron motion in a strong magnetic field. This fundamental detection principle (resonant absorption and emission of energy at a characteristic frequency) places this technique into the company of other resonance RF spectroscopies like NMR, electron paramagnetic resonance (EPR), microwave, and nuclear quadrupole resonance.

All FT-ICR instruments have four main components in common. These are the need for a strong magnet, an analyzer cell, an ultra-high vacuum system, and a sophisticated data system. Only a short description of each will be given since each component in its own right could fill a chapter. The magnet can be either a permanent magnet, an

electromagnet, or more commonly, a superconducting magnet. The performance of the FT-ICR instrument improves as the magnetic field strength increases (discussed later). Superconducting magnets have field strengths that commonly range from 3 to 9.4 tesla. As magnet technology improves so does the field strength and with this comes an increase in the performance of FT-ICR MS.

The second component is the analyzer cell. This is the heart of the instrument where ions are stored, mass analyzed, and detected. Several analyzer cell designs have been developed with specific tasks in mind, but the first, and possibly the most common design, is the cubic cell. It is composed of six plates arranged in the shape of a cube. The cell is situated in the heart of the magnetic field with one opposing pair of plates orthogonal and two pair of plates parallel to the magnetic field. The plates that are perpendicular to the magnetic field are referred to as the trapping plates. The two remaining pairs of plates are used to excite and detect the ions. Figure 1 depicts a basic cubic analyzer cell used in FT-ICR MS. A recent review presents the relative advantages of several analyzer cell designs.[19]

The third feature is the need for an ultra-high vacuum system. The performance of the FT-ICR instrument is more sensitive to pressure than other mass spectrometers. An ultra-high vacuum (pressures on the order of 10^{-9}-10^{-10} Torr) is required to achieve ultra-high resolution. To achieve these extremely low pressures, cryogenic or turbo-molecular pumps (backed by mechanical pumps) are typically preferred rather than oil diffusion pumps.

7
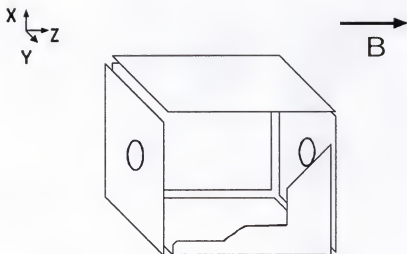
Figure 1. Schematic representation of a typical cubic trapped analyzer cell commonly used in FT-ICR MS. The three pairs of parallel electrodes and their orientation with respect to the magnetic field are depicted.

The final feature is the need for a very sophisticated data system. Some of the major components of the data station are a frequency synthesizer, delay pulse generator, broadband RF amplifier and pre-amplifier, a fast transient digitizer, and a powerful computer to coordinate all of the electronic devices during the acquisition of data, as well as to process and analyze the data. The FT-ICR technique has benefitted tremendously from the rapid growth and development of the semiconductor industry and will continue to benefit as new technological breakthroughs are made.

Motion of Trapped Ions

Cyclotron Motion

Ion cyclotron resonance spectrometers are based on the principle of cyclotron motion, by which the orbital movement of charged particles in an applied magnetic field can be described. How these charged particles are produced will be discussed later. In a strong magnetic field, a charged particle will experience an inwardly directed force known as the Lorentz force *if* that charged particle has some velocity component that is perpendicular to the direction of the field. In the absence of an electric field, the expression for the calculation of the Lorentz force experienced by an ion is given by

$$F_L = qv \times B \tag{2}$$

where q is the charge of the ion, v is the ion's velocity, and B is the magnetic field strength. The cross product in eq 2 indicates that only those velocity components perpendicular to the magnetic field contribute to the Lorentz force. Figure 2 illustrates how the Lorentz force acts perpendicular to both the velocity and the magnetic field, resulting in a circular orbit of the charged particle. The centrifugal force for an object undergoing circular motion is given by

$$F_C = mv^2/r \tag{3}$$

where *m* is the mass of the particle, *v* is the velocity of the particle, and *r* is the distance of

the object from the center of rotation.
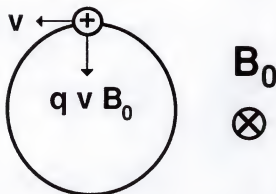
Figure 2. Origin of ion cyclotron motion. The path of an ion moving in the plane of the paper is bent into a circular orbit by the inward-directed Lorentz magnetic force produced by a magnetic field directed perpendicular to the plane of the paper. (Taken from reference 6)

When the centrifugal force is equal to the Lorentz force, the ion achieves a stable

circular orbit and Eqs 2 and 3 can be equated (in a simple treatment of the theory of ion

motion) as demonstrated by

$$mv/r = qB \qquad (4)$$

The quantity *v/r* in Eq 4 is equal to the angular frequency, ω, which is the number of

radians swept out by the ion per unit time. By substitution of this expression into Eq 4 and rearranging the terms, the well-known cyclotron equation is obtained

$$\omega_c = qB/m \qquad (5)$$

Angular frequency (radians per second) can be converted to linear frequency (cycles per second) by dividing by 2π. Finally, the celebrated cyclotron equation expressed in terms of SI units is given by

$$v_c = qB/2\pi m \qquad (6)$$

Eq 6 demonstrates that a group of ions with a given m/z always exhibit cyclotron motion at the same frequency v_c (for a given value of B). This result is one of the reasons that FT-ICR is capable of measuring spectra with ultra-high mass resolving power. Additionally, the m/z of an ion is determined from its cyclotron frequency, and since frequency is the most accurately measured physical quantity,[20] FT-ICR provides a very accurate method for m/z determination.

Trapping Motion

Cyclotron motion is one of three natural motions an ion possesses as a result of being trapped by static magnetic and electric fields. A static magnetic field applied along the z-axis effectively confines ions in the x- and y-axes according to the cyclotron motion just described. However, ions are still free to escape in the z-axis, parallel to the

magnetic field. In order to mass analyze ions they must be trapped. Trapping of ions is accomplished by the use of a Penning ion trap, or as it is more commonly known in the FT-ICR MS community, an analyzer cell (described in the previous section). Trapping is generally accomplished by applying a small (~1 volt) electrostatic potential (same polarity as the ions of interest) to each of the two trapping electrodes (trapping plates). The ion trapping frequency has been previously derived.[6] The result is given by the expression

$$\omega_T = (2\alpha q V_T/ma^2)^{\frac{1}{2}} \tag{7}$$

where α is a constant that depends on the cell geometry, q is the charge of the ion, V_T is the trapping voltage, m is the mass of the ion, and a is a characteristic trap dimension, which in the case of a cubic cell is the length of one side. In general, the trapping frequency is much smaller than the ICR orbital frequency (see Figure 3).

Magnetron Motion

The third natural motion is the "magnetron" motion which results from the relatively mass-independent precession of an ion along a path of constant electrostatic potential. Magnetron motion arises in a natural way as one of two solutions to the equations of (transverse) motion of an ion in static electric and magnetic fields. Although this motion can be excited, either intentionally or as an unintentional consequence of cyclotron excitation, it can be ignored in most FT-ICR applications.
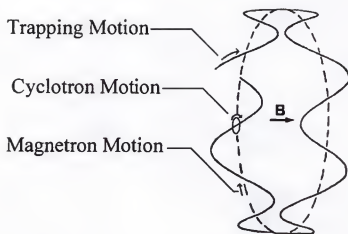
Figure 3. Schematic diagram of the natural motions of an ion trapped by a uniform magnetic and static electric field: ω_c (cyclotron), ω_T (trapping), and ω_m (magnetron). The magnetron motion is circular about a guiding center that follows a contour of constant electric potential. (Adapted from reference 21)

Experimental Procedure

The FT-ICR mass spectrometer operates in a very different fashion than most other types of mass spectrometers. With this technique, the principal functions of ionization, mass analysis, and ion detection occur in the same space (the analyzer cell) but are spread out in time, whereas with quadrupole and magnetic sector mass spectrometers, these events occur simultaneously and continuously in different parts of the mass spectrometer. The basic series of events that occur in FT-ICR MS are referred to as a pulse sequence and consists of four events: quench, ion formation, ion excitation, and ion detection. This sequence of experimental events is depicted in Figure 4. The quench

event is used to empty the analyzer cell of any ions that may be present from a previous experiment. This is accomplished simply by applying antisymmetric voltages to the trapping plates. Under these conditions, ions are axially ejected (along the z-axis) from the cell in less than 1 ms (+10 and -10 V applied to the trapping plates).

BASIC PULSE SEQUENCE
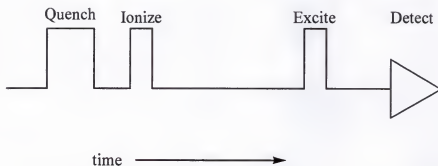
Figure 4. A general experimental pulse sequence that illustrates the four fundamental steps needed in order to obtain a mass spectrum using FT-ICR MS.

Ion Formation

Samples to be analyzed can be either a solid, liquid, or a gas. There are several possible techniques to get these samples into the gas. Solids probes are used to introduce solids of sufficient vapor pressure into the vacuum chamber, while leak valves and/or pulsed valves are used for liquids and gases. Once the samples are in the vacuum chamber, FT-ICR MS detects ions, therefore the samples need to be ionized. There are many different techniques that are used to ionize a sample depending on the specific

needs of the mass spectrometrist and the sample that is to be analyzed. These include (in no particular order) electron impact ionization (EI)[22], chemical ionization (CI)[23], laser desorption (LD)[24-27], plasma desorption (PD)[28,29], electrospray ionization (ESI)[30-34], fast atom bombardment (FAB)[35], secondary ion mass spectrometry (SIMS)[36], field desorption (FD)[37-40], and matrix-assisted laser desorption (MALDI).[41-43] Two of these ionization techniques (EI and ESI) will be discussed in more detail in later chapters. Appropriate references are cited for a more detailed discussion of each of the remaining techniques.

Ion Excitation

The ICR orbital motion that results from the magnetic and electric fields does not by itself generate an observable electrical signal. At its instant of formation the phase of each ion's orbital motion is random. In other words, an ion may start its cyclotron motion at any point along the circle depicted in the left diagram of Figure 5. Thus, any charge induced in either of the two opposed detector plates will be balanced, on the average, by an equal and opposite charge induced by an ion whose phase is 180° different.

To circumvent the aforementioned problem of incoherency, the first step in FT-ICR MS detection is to excite the ions. There are several excellent references that discuss the fundamental process of excitation in FT-ICR.[44-46] In order to create a signal on the detector plates, an ion packet whose cyclotron orbits are initially centered on the z-axis must be made spatially coherent by moving the ion packet off-center. This is accomplished by applying an oscillating resonant phase-coherent electric field excitation that accelerates the ions of interest into larger cyclotron orbits. An ion's orbital radius
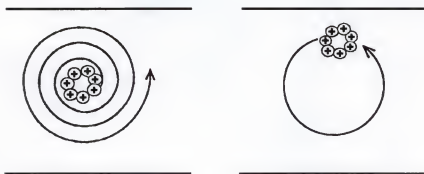
Figure 5. Incoherent ion cyclotron orbital motion (left) is converted to coherent (and therefore detectable) motion (right) by the application of an oscillating voltage to the excitation plates. Ions which are in resonance with the excitation frequency gain kinetic energy and spiral outward from the center of the cell into a larger cyclotron orbit (right). (Taken from reference 6)

can be determined from the following expression

$$r = 1/qB\,(2mkT)^{\frac{1}{2}} \tag{8}$$

where q is the charge on the ion, B is the applied magnetic field strength, m is the mass of the ion, k is the Boltzmann constant, and T is the temperature of the ion. The previous equation can readily be derived from Eqs 4 and 9 which relates the translational energy of an ion to its temperature

$$kT = mv_{xy}^2/2 \tag{9}$$

As shown in Eq 8, the cyclotron radius of an ion can be increased by increasing its temperature (its kinetic energy). In addition to increasing an ion's cyclotron radius, excitation simultaneously achieves spatial coherency. The RF electric field component rotating in the same sense (in resonance with) as the ion of interest will push that ion continuously forward in its orbit. Thus, ions can be excited to detectable ICR orbital radii by a relatively small RF electric field. Therefore, all ions of a given m/z range can be excited to the same ICR orbital radius, by application of an RF electric field whose magnitude is constant with frequency.

The goal for excitation is usually to excite all of the ions in the mass spectral range of interest to the same cyclotron orbital radius to produce a flat spectrum without mass discrimination. Several methods of ion excitation have been developed that achieve these conditions. The effects of an excitation waveform can be evaluated by displaying the excitation spectrum. This is obtained by performing an FT on the time-domain excitation waveform. The excitation spectrum portrays the amount of excitation at any frequency or mass, from which parameters such as ion radius, ion excitation energy for MS/MS, and overall evenness of the excitation can be observed. The three most common types of excitations are impulse excitation,[6,47,48] chirp excitation,[17,45,49] and stored waveform inverse Fourier transform (SWIFT) excitations.[50] All three of these excitation methods have been discussed in detail elsewhere and only a brief description of each will be given.

Impulse excitation

An ideal delta function pulse (infinite amplitude, zero width) has a flat excitation spectrum and should excite all of the ions equally. In real world approaches to this idea a pulse of finite width and height is used (see Figure 6a). The shape of the pulse is not very important. The mass range of ions that are excited extends from infinite mass to a lower limit mass whose angular cyclotron frequency is of the order of $\omega_{c,max} = 1/t$, where t is the pulse width. McIver et al.[47] have discussed the quantitative aspects of impulse excitation and have shown that it is useful with a pulse amplifier delivering peak pulse amplitudes of the order of 1 kV.[48]

Chirp excitation

The most commonly used excitation waveform is the "chirp", an RF pulse whose frequency sweeps rapidly over the range from the lowest to the highest (or highest to lowest) frequencies desired in the spectrum (see Figure 6b). A fairly flat excitation spectrum results if the frequency sweep traverses a constant number of Hertz per second. The mathematics of the FT with a chirp are slightly complicated, but were formulated long ago (see reference 6). The advantages of chirp excitation are its rather simple implementation and the ease with which a wide mass range can be excited without the need for large RF amplitudes and expensive amplifiers. Disadvantages are the somewhat nonuniform excitation of the ions, which becomes pronounced for ions near the edge of the swept frequency range (depicted in Figure 6b).
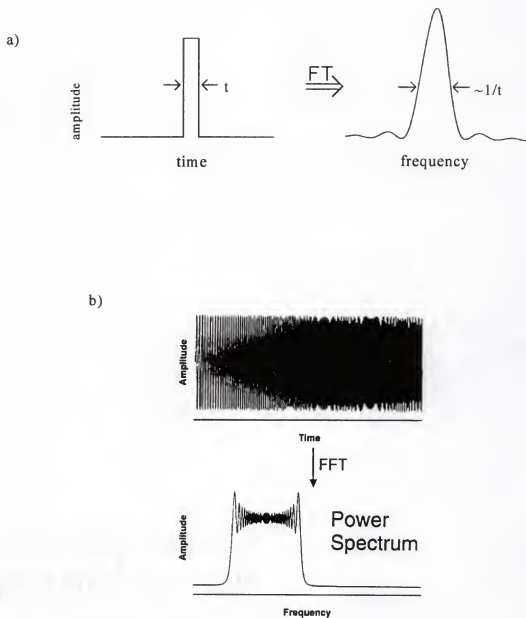
Figure 6. A Fourier excitation waveform and excitation spectrum for impulse (a) and chirp (b) excitation. (Taken from reference 7)

SWIFT excitation

In 1985, Marshall and coworkers introduced the SWIFT excitation method, which is the most satisfactory approach to achieving complete control over the excitation characteristics to date.[50-52] It is based on the fact that the excitation that is actually experienced by each ion, and therefore its final radius, is proportional to the amplitude of the excitation spectrum at its frequency. Recalling that the excitation spectrum is produced via an FT of the excitation waveform, a desired excitation waveform can be produced via an inverse FT of the excitation spectrum. The SWIFT technique specifies the excitation spectrum actually desired for the excitation waveform. This is ordinarily a square shape that extends the desired frequency range, as in Figure 7a. It can, however, just as well be a complicated shape with gaps, changing amplitudes, and other features as depicted in Figure 7b. The specified excitation spectrum is inverse Fourier-transformed to give the time-domain excitation waveform, as depicted in the right side of Figures 7a and 7b. If carried out precisely, this gives an excitation waveform that will excite each ion to exactly its preselected cyclotron radius.

Ion Detection

Detection in FT-ICR MS is based upon the principle of electric induction, whereby a current flows through a circuit in response to an accumulation of charge. The current will always flow in such a way that seeks to minimize the charge buildup. All ions of the same m/z are excited coherently and undergo cyclotron motion as a packet. As the orbiting ion packet passes the cell's electrodes (the detection plates), the coherent orbiting ion packet attracts electrons to first one and then the other of the two detection
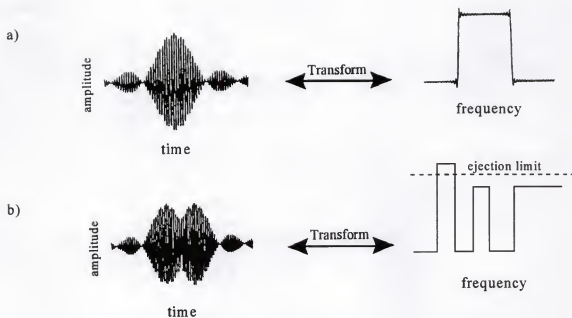
Figure 7. An illustration of the principles of SWIFT excitation (a) and a SWIFT excitation depicting selective ejection of unwanted ions (b). (Taken from reference 7)

plates through external circuitry (see Figure 8). This alternating current is referred to as the image current.[53] The periodic cyclotron motion of the ions produces a sinusoidal image signal which can be amplified, digitized, and stored for processing by a computer. The frequency of the detected sinusoid is nearly equal to the frequency of the cyclotron motion of the ions; it is exactly equal to the difference between the cyclotron and magnetron frequencies.
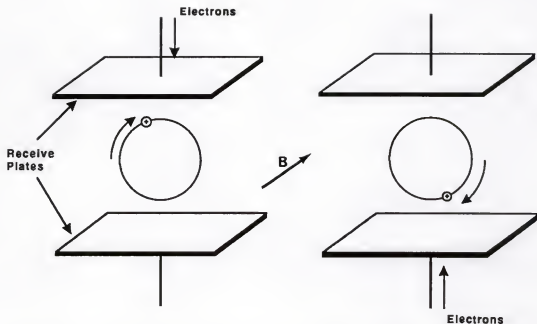
Figure 8. A rotating monopole description of signal generation. Positive ions approach one plate, attracting electrons. As the ions continue moving in a circle, they approach the other plate and attract electrons. Thus, the ion motion induces a small AC (sine wave) current, an image current, in the detection plates. (Taken from reference 7)

Image current detection provides unique capabilities for FT-ICR MS. All other mass spectrometers detect ions by destructive collisions with an electron multiplier. Image current detection is non-destructive; the ions remain in the analyzer cell after the detection process has been completed. Since ion detection is nondestructive, ions can be repeatedly detected many times which improves the signal-to-noise ratio (S/N) since the ion signal increases as the square root of the number of detection events. Finally, the image current is converted to a voltage, amplified, digitized, and Fourier transformed to

yield a frequency spectrum that contains complete information about frequencies and abundances of all ions trapped in the cell. Finally, a mass spectrum can then be produced by converting frequency into mass (see Eq 6). Because frequency can be measured precisely, the mass of an ion can be determined to one part in 10^9 or better.
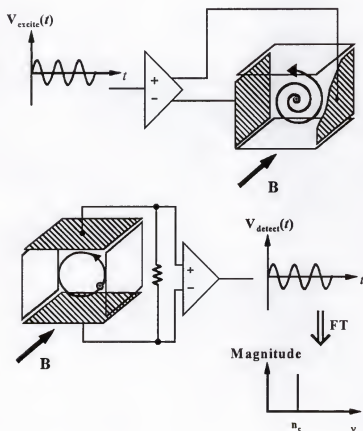
Figure 9. Overall depiction of an FT-ICR mass spectrometer. The upper diagram depicts the excitation of the ion packet by an externally applied alternating RF field. The lower picture shows the detection of the image current that is produced by the coherently orbiting ion packet on the two opposing detection plates to produce a time-domain signal. The time-domain signal is then converted to a voltage, digitized, and Fourier-transformed to yield a frequency-domain spectrum which is then converted to a mass spectrum. (Adapted from reference 54)

Conclusion

The purpose of this chapter was to provide the reader with a general summary of the FT-ICR technique, from its roots in the 1930s to the modern day instrument. Even after its relatively short existence (roughly some 25 years), FT-ICR MS has proven itself to be the method of choice for many researchers who are interested in the unique qualities this technique has to offer. The mass resolution and mass accuracy achieved by FT-ICR mass spectrometers is much higher than any other type of mass spectrometer. The technology has come to a point where even pharmaceutical and biotechnology companies are now employing the use of FT-ICR mass spectrometers to assist them in their everyday analysis of samples. With future advancement of higher magnetic fields (at the National High Magnetic Field Laboratory and Battelle Pacific Northwest National Laboratory) as well as more powerful computers, improvements in not only mass resolution and mass accuracy but also in mass range, will undoubtedly make this technique *the* choice of mass spectrometrists in the future.

CHAPTER 2
GAS PHASE BINDING ENERGIES OF SELECTED
HOST:GUEST COMPLEXES

Introduction

Gas phase binding energies of a series of amino acids trapped within the cavity of cyclodextrin molecules were measured using FT-ICR MS. To begin the chapter, a brief background regarding cyclodextrins will be offered. This is followed by a description of the experimental procedures that were applied; namely electrospray ionization and collision-induced dissociation. Finally, a discussion regarding the results obtained from these experiments along with a few comments on possible future experiments will be presented.

Cyclodextrin Background

Cyclodextrins (CDs) encompass a family of cyclic oligosaccharides that are produced from the enzymatic degradation of starch. The first reference to a substance that was later proven to be a CD was that of Villiers[55] in 1891. Villiers successfully isolated a white crystalline compound after digesting starch with the enzyme *Bacillus amylobacter*. It would be over ten years before a detailed report was published by Schardinger[56] that characterized the preparation and isolation of CDs. Schardinger was investigating strains of bacteria that were thought to be responsible for certain types of food poisoning that were occurring near the turn of the century. After digesting the starch

24

with such a microorganism, he was able to isolate small amounts of two different crystalline compounds which appeared to be identical with the "cellulosines" reported by Villiers a decade earlier. Schardinger named the isolated microbe *Bacillus macerans*.[57,58] It was determined much later that, during the preparation process, the starch helix is hydrolyzed, and its ends are joined together through α-1,4 linkages.[59,60] The enzymes that are used in the digestion of starch are not specific as to the site of hydrolysis resulting in a product that exhibits a number of different cyclic and linear dextrins.

Investigations into the chemistry of CDs have increased for several decades. Literature regarding structures, properties, and applications of CDs have been the subject of several books,[61-67] a number of review articles,[68-84] more than 800 patents, and countless papers in the years up to 1992. Their physical and chemical properties contribute to the broad interests from different scientific disciplines. CDs are the first and probably the most important examples of relatively simple organic compounds which exhibit complex formation with other organic molecules. They are excellent models of enzymes which led to their use as catalysts (for both enzymatic and nonenzymatic reactions), and they are natural products that are readily available to most researchers.

The three most common CDs possess six, seven, and eight glucose units and are referred to as α-, β-, and γ-cyclodextrin, respectively. CDs that contain fewer than six glucose units are too strained to exist[85] whereas those that have more than eight are very soluble and difficult to isolate (though they have been identified by column chromatography).[86] The chemical structures of the three most common CDs are depicted in Figure 10 while Figure 11 shows the glucose units in the relatively undistorted C_1 chair
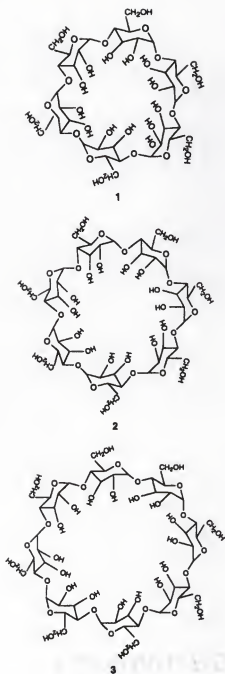
Figure 10. Compounds 1-3 are the chemical structures of the three most common cyclodextrins: α-, β-, and γ-cyclodextrin, respectively.
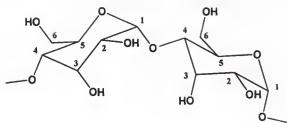
Figure 11. Portion of a cyclodextrin molecule showing the glucose units connected through glycosidic α-1,4 linkages.

conformation as well as the α-1,4 linkages. This arrangement allows the CD to maintain an overall shape of a ring, or more accurately a conical cylinder, which is often described as a doughnut or wreath-shaped truncated cone. The wider side of the cone is created by the secondary 2- and 3-hydroxyl groups while the narrower side is created by the primary 6-hydroxyl group (see Figure 10). The number of glucose units in the ring governs the overall dimensions of the cavity, as depicted in Figure 12. The cavity is lined with the hydrogen atoms and the glycosidic oxygen bridges. The nonbonding electron pairs of the glycosidic oxygen bridges are directed toward the interior of the cavity providing high electron density along with Lewis base characteristics. As a result of this arrangement of functional groups in the CD molecules, the cavity is relatively hydrophobic (compared to water) while the external faces are hydrophilic. Moreover, a ring of hydrogen bonds is also formed intramolecularly between the 2-hydroxyl and the 3-hydroxyl groups of adjacent glucose units. This hydrogen bonding ring gives the CD a remarkably rigid structure.
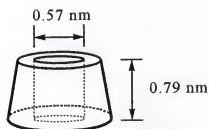
α-cyclodextrin ($C_{36}H_{60}O_{30}$), cavity volume 0.202 nm^3
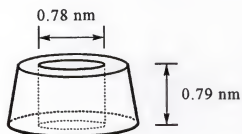
β-cyclodextrin ($C_{42}H_{70}O_{35}$), cavity volume 0.377nm^3
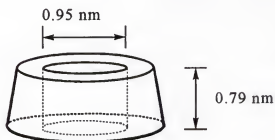
γ-cyclodextrin ($C_{48}H_{80}O_{40}$), cavity volume 0.560 nm^3

Figure 12. Representation of the three most common cyclodextrins (α-, β-, and γ-cyclodextrin) along with approximate dimensions and cavity volumes.

It is the cavity that generates the attraction of many disciplines to the chemistry of CDs. As a result of the polar exterior and the relatively nonpolar interior, these compounds have been studied as "host" molecules for the inclusion of "guest" molecules which are capable of entering the cavity. The unique properties of the CD cavity explain some of the unusual features of these molecules; thus, they form inclusion complexes rather unspecifically with a wide variety of guest molecules. The only obvious requirement for the guest molecule is that it must fit into the cavity, even if only partially. Based on this fact, it is not surprising to find that organometallics,[87] amino acids,[88-90] peptides,[88,91-93] aromatic molecules,[94] drugs,[95,96] explosives,[97] and metal ions[98] are included, just to name a few in a long list of potential host species.

The evolution of host-guest chemistry started in 1967 with the discovery of crown ethers by Pedersen.[99,100] The term "host-guest chemistry" has been used to designate a variety of processes occurring in a number of research fields, such as organic, analytical, biological, pharmaceutical, and organometallic chemistry, and involving molecules and ions of different structures, dimensions, and properties. Restricting the definition of host-guest chemistry by considering the common elements that these disciplines possess is possible. In general, host-guest interactions involve the establishment of multiple non-covalent bonds between a large and geometrically concave organic molecule (the host) and a simpler organic or inorganic molecule or ion (the guest). Guest molecules or ions can be fully entrapped within the cavity or partially trapped as is the case with larger species such as peptides and proteins. Table 1 lists cavity dimensions as well as other properties of interest for the three most common CD molecules.

Table 1. A brief listing of selected physicochemical properties of the three most common cyclodextrin molecules. (Adapted from reference 101)

property	cyclodextrin		
	α	β	γ
no. glucose units	6	7	8
empirical formula (anhydrous)	$C_{36}H_{60}O_{30}$	$C_{42}H_{70}O_{35}$	$C_{48}H_{80}O_{40}$
mol. wt. (anhydrous)	972.85	1134.99	1297.14
cavity length, Å	7.9	7.9	7.9
cavity diameter, Å (approx.)	~5.7	~7.8	~9.5
α_D, deg.	+150.5	+162.0	+177.4
heat capacity (anhydrous solid), J mol^{-1} K^{-1}	1153	1342	1568
heat capacity (infinite dil'n.), J mol^{-1} K^{-1}	1431	1783	2070
pK_a (25°C)	12.33	12.20	12.08
ΔH^o (ionization), kcal mol^{-1}	8.36	9.98	11.22
ΔS^o (ionization), cal mol^{-1} K^{-1}	-28.3	-22.4	-17.6
solubility (water, 25°C), mol L^{-1}	0.1211	0.0163	0.168
ΔH^o (solution), kcal mol^{-1}	7.67	8.31	7.73
ΔS^o (solution), cal mol^{-1} K^{-1}	13.8[a]	11.7[a]	14.7[a]

[a]Mole fraction standard state.

In aqueous solution, the slightly apolar CD cavity is occupied by water molecules, which is energetically unfavorable, and therefore, the cavity can be readily substituted by appropriate guest molecules which are less polar than water molecules. The dissolved CD is the host molecule with the driving force of complex formation being the substitution of the high-enthalpy water molecules by an appropriate guest molecule. Most frequently, the host:guest ratio is 1:1; this is the basis of "molecular encapsulation." A 1:1 ratio is the most common case; however, 2:1, 1:2, 2:2, or even more complicated associations and higher order equilibria exist, almost always simultaneously. How these CD molecules are promoted into the gas-phase for analysis by mass spectrometry will be presented next.

Electrospray Ionization

Recent advances in the biological sciences have generated a tremendous demand for the characterization of large biopolymers including peptides, proteins, oligonucleotides, and oligosaccharides. There has been tremendous pressure on the analytical chemistry community to keep up with these advances. A few of the daily challenges that are required of modern instrumentation are the need for rapid determination of molecular weight, purity, sequence, and site and nature of modifications. The biological sciences have greatly benefitted in recent years from improvements that have been made in mass spectrometry. More than ever, mass spectrometry has been called upon for the investigation of biopolymers because it does not suffer from certain limitations of the classical techniques[102] such as gel electrophoresis or Edman degradation. The single event that finally demonstrated the usefulness of mass spectrometry for the biological sciences was the development of a new ionization technique. Historically, conventional mass spectrometric methods could only be used on low molecular weight, volatile compounds. Larger species simply could not be promoted into the gas phase without undesirable degradation and/or fragmentation. Since the inception of electrospray ionization (ESI), the upper limit to molecular weight of proteins and biopolymers which can be studied has continued to increase to well over 100,000 kDa.

The capability to impart multiple charges upon an analyte molecule is the principal feature of ESI that distinguishes it from other ionization techniques. These highly charged molecular ions, which normally exhibit little or no fragmentation, are reduced to a m/z range where conventional mass spectrometers routinely operate. The

combination of this fact along with the advantages of FT-ICR MS discussed previously, makes ESI FT-ICR MS quite possibly the most powerful analytical technique for studying very large proteins, biomolecules, or biopolymers. An example of the power of this coupling of techniques has been reported by Smith *et al.*[103] They recently reported the mass spectrum of a protein, bovine serum albumin (MW 66,430 Da), which showed ions with a charge distribution of +30 to +50 that corresponded to m/z values ranging from 2214 to 1329, respectively. Electrospray ionization-mass spectrometry has been used to study a wide range of systems including proteins and glycoproteins,[104] nucleotides (including DNA, RNA, and oligonucleotides),[105] fullerenes,[106] synthetic polymers,[107] and inorganic transition metal complexes.[108]

Yamashita and Fenn[33,109] were the first to demonstrate electrospray mass spectrometry (ESMS) which was based upon the pioneering work of Dole *et al.*[30] The dramatic impact of this new technique was slow to be realized by most in the scientific community.[110-112] After several years of proven success and universal acceptance of the ESMS technique, much attention has now turned to understanding the mechanism of gas-phase ions production from solution phase analytes. There are at least three essential steps to consider: creation of charged droplets from dissolved electrolytes; solvent evaporation that leads to charged droplet shrinkage followed by repeated droplet disintegrations (fissions); and the mechanism of gas-phase ion production from small, highly charged droplets. A brief description of the three processes is presented below.

Production of Charged Droplets

The ES events are depicted in Figure 13. A voltage of 2-3 kV is applied to a small metal capillary (typically 0.2 mm o.d. and 0.1 mm i.d.) which is normally located from 1 to 3 cm from a larger planar counter electrode. The counter electrode will have an opening that leads to the mass spectrometric sampling system in most ESMS applications (for example, this opening allows ions to be transferred to the analyzer cell in FT-ICR MS). Due to the size of the capillary tip, the electric field in the atmosphere surrounding the tip is very high ($E \approx 10^6$ V m^{-1}). When the capillary of radius r_c is located at a distance d from the planar counter electrode, the magnitude of E_c for a given potential V_c is given by[113,114]

$$E_c = 2V_c/r_c \ln(4d/r_c)$$ (10)

This equation provides the field at the capillary tip in the absence of solution. The electric field is proportional to the applied potential while the dominant geometric parameter is the capillary radius.

Typical solutions used in ESMS will consist of a dipolar solvent in which electrolytes are at least fairly soluble. Methanol (or methanol/water) is generally the solvent of choice with small amounts of acetic acid added as the source of electrolytes. For optimum operation of ESMS, low electrolyte concentrations (10^{-6}-10^{-4} M range) are required. The choice of solvent, solvent mixtures, solvent mixture ratios, and
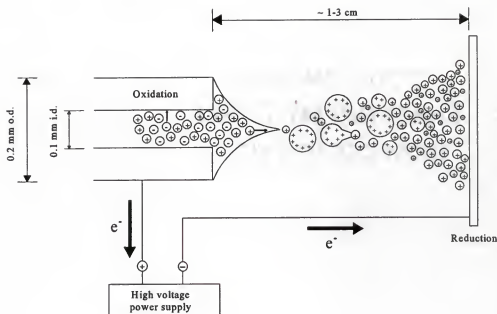
Figure 13. A simple depiction of the processes that occur in electrospray mass spectrometry. (Adapted from reference 115)

concentrations are, of course, parameters that can be different depending on the specific system of interest and which would need to be characterized for optimum efficiency.

The applied electric field partially penetrates the liquid at the capillary tip. If the capillary is the positive electrode, the negative ions in the liquid will migrate toward the electrode while the positive ions migrate toward the liquid surface until the imposed field inside the liquid is essentially removed by this charge redistribution. Negative ions can also be generated for further investigation if the capillary is the negative electrode. The

accumulation of positive charge at the liquid surface tends to destabilize the liquid surface since the positive ions are repelled down field but cannot escape from the liquid. The surface is drawn out such that a liquid cone forms which has been referred to as a Taylor cone[116] in honor of Sir Geoffry Taylor.

Eventually, as the electric field is increased above a certain value, the cone becomes unstable, resulting in a liquid filament with a diameter of a few micrometers (with a surface enriched with positive ions) being emitted from the cone tip. Separate droplets are formed downstream as the liquid filament becomes unstable with a continual increase of the electric field. The droplet surfaces are enriched with positive ions for which there are no negative counterions. The length of the unbroken liquid filament will decrease if the electric field is increased.

Charged Droplet Shrinkage

Since the initial size and the number of charges on the droplets depend on the spray conditions, it will be convenient for the next discussion to consider droplets that are formed by low flow rates (~5 μL min^{-1}) and concentrations that are less than 10^{-3} M. Droplets formed by these conditions are considered to be monodisperse since they are small and have a narrow distribution of sizes. It has been shown that the size distribution peaks at a radius of about 1.5 μm while possessing a charge on the order of 10^{-14} C, which corresponds to approximately 50,000 singly charged ions.[117,118]

The conditions that determine when the charge, Q, becomes sufficient to overcome the surface tension, γ, that holds the droplet together are given by the Rayleigh equation[119]

$$Q^2_{\mathrm{R}} = 64\pi^2\varepsilon_o\gamma R^3_{\mathrm{R}} \tag{11}$$

where ε_o is the permittivity of vacuum and R_{R} is the Rayleigh radius.

Larger droplets (within the micrometer range or larger) maintain their charge and do not emit gas-phase ions.[118,120,121] After the droplets have decreased in size to near the Rayleigh limit, they become unstable and begin to divide (undergo fission) into smaller droplets as seen in Figure 14. Studies have shown that the droplets do not produce offspring droplets of equal size and charge.[118,120,121] Furthermore, it was observed that the droplets tend to vibrate alternately from prolate to oblate shapes. These vibrations cause disruptions where the droplet releases a tail of much smaller offspring droplets. The offspring droplets take about 15% of the original charge and nearly 2% of the original mass with them when they are emitted. The radius of the offspring droplets is about one-tenth that of the parent droplets.[118,122,123] The total time for this sequence of events is in the hundreds of microseconds as seen from Figure 14 (calculated using methanol).

Mechanism of Gas-Phase Ion Production

Over the years, two different mechanisms have been proposed to account for the formation of gas-phase ions from the charged droplets. Dole *et al.*[30] devised the first mechanism which involved the formation of extremely small droplets ($R \approx 1$ nm) that feature only one ion. Their mechanism allows gas-phase ions to evolve directly from these extremely small, solvent-evaporated droplets. How these extremely small droplets were formed or whether the process should include selectivity that may favor the formation of gas-phase ions A^+ relative to B^+ was not addressed in their proposal.
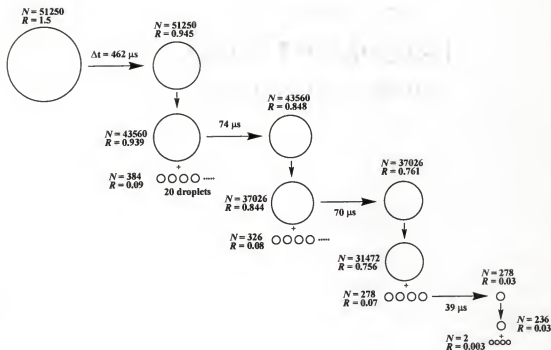
Figure 14. Schematic representation of the ion evaporation model based on methanol as the solvent. The parent droplet that is created at the spray tip undergoes uneven fission as time passes. The depiction demonstrates how the parent droplet shrinks (losing about 2% of its mass) and loses charge (approximately 15%) as it produces daughter droplets while drifting toward the counter electrode. (Adapted from reference 115)

The second mechanism, proposed by Iribarne and Thomson,[124,125] assumed that ion evaporation resulted from very small and highly charged droplets. Normally, the droplets have a radius of about 8 nm and roughly 70 elementary charges[124,125] when ion emission becomes competitive with Rayleigh fission. At this point, the droplet releases gas-phase ions rather than undergo fission to produce yet smaller droplets. As the

number of charges decrease, emission is still possible as a result of a decrease in the radius of the droplets by solvent evaporation. Thus, the Iribarne mechanism does not require the production of extremely small droplets that contain only one ion (as in Dole's theory). Iribarne emission can occur even when the droplet contains other solutes such as charge-paired electrolytes. At present, it is not possible to state with certainty which theory fits better with the available evidence.

Collision-Induced Dissociation

The goal of this project was to ascertain the gas-phase binding energies of a series of amino acids that were trapped within the cavity of CD molecules. The previous discussion pertained to the generation of gas-phase ions; next a short discussion on how the binding energies were determined will be presented.

Several different techniques have been developed for ion structure determination, but collision-induced dissociation (CID) remains one of the most useful and widely implemented mass spectrometric techniques, especially when employed in an MS/MS technique for complex mixture analysis.[126-128] Basically, this technique consists of isolating an ion of a specific mass, accelerating the chosen ion, and allowing it to pass through a collision gas. Upon collision, some of the ion's kinetic energy is converted into internal energy. This allows for a faster redistribution of energy throughout the normal modes allowing for higher energy fragmentations to occur. Normally, high kinetic energies (3-30 keV) are required to observe CID using mass-analyzed ion kinetic energy spectrometry (MIKES) in reverse-geometry mass spectrometers.[126-128] But Yost and Enke[129] were able to show that a low-energy (10-200 eV) CID process was possible with

high efficiency by using a triple-quadrupole mass spectrometer. This low energy pathway is readily accessible with an ICR spectrometer using the double-resonance technique to irradiate a given ion at its cyclotron frequency in order to accelerate it. The amount of kinetic energy transferred to the ion is limited to being less than that required to totally eject the ion from the cell, typically 10-1000 eV. As long as a collision gas is used at a sufficiently high pressure ($\sim 10^{-5}$ Torr), dissociation may be observed instead of the ejection of the ion from the analyzer cell. Thus, their quadrupole results suggested that CID should be feasible in an FT-ICR mass spectrometer. In fact, CID was reported in the literature using conventional ICR mass spectrometers well before the quadrupole results appeared[130-133] but received little attention and remained essentially a curiosity. A possible reason for the lack of interest was due to the cumbersome nature of the experimental procedure for a conventional ICR mass spectrometer.

The infinite parallel plate capacitor approximation[134,135] (given in Eq 12) has commonly been used to calculate the translational energy imparted to an ion during the excitation stage of the FT-ICR CID process

$$E_{ion} = q^2 V^2 t^2 / 8md^2 \tag{12}$$

where q is the charge of the ion, V is the amplitude of the RF excitation pulse, t is the RF pulse width, m is the mass of the ion, and d is the distance between the excitation plates of the analyzer cell. However, since the actual analyzer cell in many cases is a cubic cell, and therefore not an *infinite* parallel plate capacitor, the electric fields and translational

energies will undoubtedly be less than those values predicted for an infinite parallel plate capacitor. In fact, calculations and ion motion simulations[136] have demonstrated that excitation of ions located at the center of a cubic analyzer cell reached a radius that was only 72% of the theoretical radius that was calculated using an infinite parallel plate capacitor approximation. The actual excitation is even less since an ion's translational energy is proportional to the square of its radius. Therefore, actual excitation is only 0.52 of that predicted by Eq 12. It is extremely important to keep the ion excitation time to a minimum. The important thing is that collisions between the ions and the collision gas occur *after* translational excitation, otherwise, uncertainties in the amount of energy actually imparted during the excitation process will result.

Some of the most dramatic and promising MS/MS applications in FT-ICR MS involve sequential dissociations in which successive fragmentation of the parent ion into smaller and smaller fragments is followed by a series of excitation/observation steps on the successive fragments.[137,138] An excellent illustration of MS^n analysis was demonstrated by Freiser and Gord,[139] where five CID steps were used, along with selective ejection, to proceed from FeS_{10}^+ down to Fe^+ (see Figure 15). Carrying such multiple MS/MS observations to four or five steps is basically equivalent to a multisector or multi-quadrupole MS/MS experiment using a long (and impractical) series of sectors or quadrupoles. This experiment illustrated the use of an FT-ICR MS as a series of temporally separated mass analyzers.

The basic CID process can be thought of in terms of two consecutive steps that occur on well-separated time scales. The first is a rapid step ($\sim 10^{-15}$-10^{-14} s) in which a

41
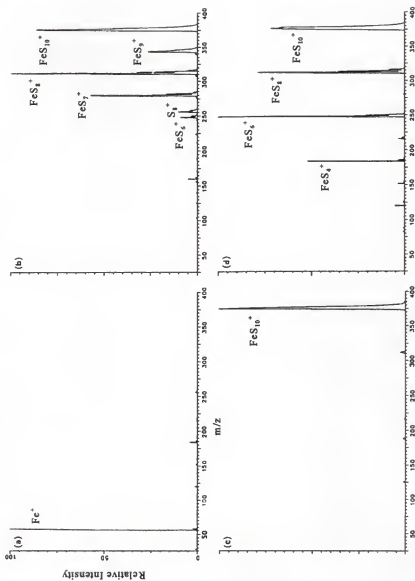
Figure 15. Resulting mass spectra following five stages of CID of FeS_{10}^{+}. (a) Isolation of Fe^{+} following laser desorption and collisional cooling with argon and S_8. (b) Reaction of Fe^{+} with S_8. (c) Isolation of FeS_{10}^{+}. (d) CID of FeS_{10}^{+}. (e) Isolation of FeS_8^{+}. (f) CID of FeS_8^{+}. (g) Isolation of FeS_6^{+}. (h) CID of FeS_6^{+}. (i) Isolation of FeS_4^{+}. (j) CID of FeS_4^{+}. (k) Isolation of FeS_2^{+}. (l) CID of FeS_2^{+}. (Taken from reference 139)
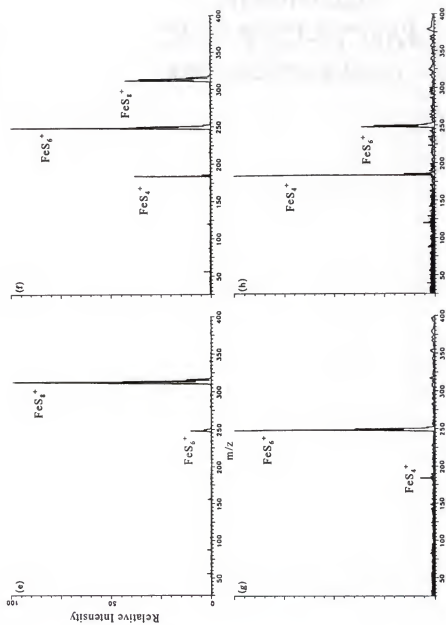
Figure 15. Continued.
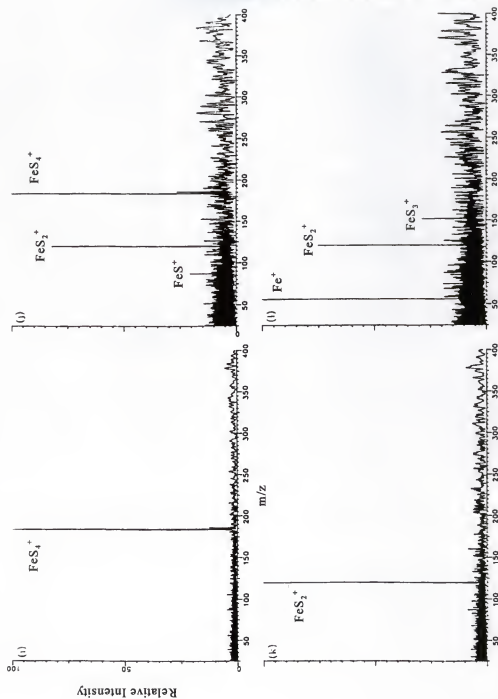
Figure 15. Continued.

small amount of the initial translational energy of the accelerated ion is changed into internal energy of both the ion and target molecule (the target molecule also acquires translational energy). The next step in this process is the dissociation of the energized (and typically isolated) ion. The yield of product ions after collisional dissociation depends on the probability of unimolecular decomposition of the precursor ion after excitation. To explain the rates of such reactions, quasi-equilibrium theory (QET) has been used.[140-144] In simple terms, the theory states that unimolecular decomposition reactions depend upon the random distribution of the internal energy of the ion among all the vibrational modes of that ion. In other words, the rate of decomposition is related to the probability of a given vibrational mode or modes acquiring enough energy to rupture bonds.[145] Since there are $3N$ - 6 vibrational modes in a nonlinear ion that contains N atoms, the number of vibrational modes will be in direct proportion to the molecular mass for a given class of compounds. Because the random distribution of internal energy among the vibrational modes is required by QET, the average energy per mode must decrease with increasing molecular mass. Because the decrease is related to the inverse of the mass of the ion, the fragment ion yield should decrease similarly beyond some threshold.

In the early days, low-energy CID mass spectra were observed in quadrupole reaction chambers of triple quadrupole or hybrid sector-quadrupole mass spectrometers, but in recent years low-energy CID has been performed more and more with FT-ICR mass spectrometers. Regardless of the choice of instrument configuration, an obvious

requirement is the presence of a collision cell that can be pressurized with a suitable target gas.

Collisions that occur at large energies (keVs) are assumed to result in excitation of electronic internal modes (and to a lesser extent rotational-vibrational modes); collisions that occur at lower energies (<100 eV) will no longer result in efficient transfer of translational energy to electronic internal modes. A typical interaction time of a selected ion of mass 200 and a translational energy of 30 eV with a target molecule over a few angstroms is on the order of 10^{-13} s. This is longer than the time needed for internal electronic excitation and thus, the probability of such excitation is reduced with respect to excitation by high-energy (keV) CID.[146]

The interaction time of ca. 10^{-13} s is comparable to the reciprocal of typical vibrational frequencies. Under these conditions, the collisions are nonadiabatic and the interaction is described as having an impulsive character that can effectively induce energy transfer.[146] The subsequent transfer of translational to vibrational energy is believed to occur by internuclear momentum transfer.[147]

In the so-called binary or spectator model, the selected ion and the target gas engage as essentially structureless elastic spheres. Momentum is transferred between the two bodies which leads to rotational-vibrational excitation of the ion, as well as the gas, along with a shift in momentum in the center of mass of each. If the ion is much larger than the collision gas, the gas will only interact with a small portion of the selected ion. The maximum amount of energy (center-of-mass kinetic energy, E_{com}) accessible for

internal excitation is given by Eq 13[148]

$$E_{com} = E_{lab}m_t/[m_p + m_t(m_p/m_{pi})] \tag{13}$$

where m_p is the projectile mass, m_{pi} is the impact portion of the projectile, and m_t is the target mass. The elastic limit is thought to be reached when $m_p = m_{pi}$.

With low-energy collisions, the composition of the target gas plays a much more important role than it does with high-energy collisions. The reason for this is that a different excitation mechanism (vibrational excitation) is at work. Furthermore, a larger portion of the maximum available energy is converted into internal energy of the target ion. Bursey and co-workers[149-151] demonstrated that heavier targets are preferred over lighter targets because they provide a larger E_{com}. They found that collisions using helium transferred very small amounts of energy when compared with collisions using nitrogen, argon, or krypton.[149,152] Specifically, for every volt change in E_{lab} of the selected ion at a given pressure, there was an increase of 0.04, 0.25, and 0.32 eV, in maximum possible energy transferred when using helium, nitrogen, and argon, respectively.[152]

Experimental

The experiments were conducted on a Bruker CMS 47X FT-ICR mass spectrometer (Bruker Daltonics, Billerica, MA) incorporating a shielded 4.7 T superconducting magnet (Magnex Scientific Limited, Abingdon, England) and a modified external electrospray ionization source (Analytica of Branford, Inc., Branford, MA). Figure 16 depicts the instrument used throughout this work. The commercially-sold glass capillary
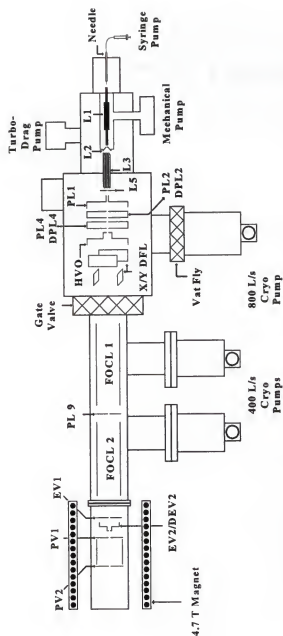
Figure 16. Fourier transform ion cyclotron resonance mass spectrometer used to determine the gas-phase binding energies of cyclodextrin:amino acid complexes. The instrument employed a shielded 4.7 T magnet, an external electrospray ionization source, and possessed three stages of differential pumping to achieve analyzer cell pressures on the order of 5.0×10^{-9} Torr.

which utilized heated N_2 for desolvation was replaced in favor of a heated metal (brass) capillary (designed and built in-house)[153] which produced a more stable ion current. The capillary utilized a cartridge heater and under normal operating conditions was heated to between 100-130°C to assist in generating desolvated gas phase ions.

The CDs (α-, β-, and γ-) and amino acids were provided by Dr. Lazslo Prokai and used without further purification. Typical solution concentrations were 10^{-4} M for the CDs and 10^{-3} M for the amino acids. The samples were sprayed from a water/methanol (50/50) solvent with a small amount of acetic acid added to provide charge. The solutions were introduced to the electrospray needle with the aid of a 74900 Series syringe pump (Cole-Parmer Instrument Company) normally operating at 60 μl hr^{-1}. The electrospray needle potential was normally maintained near +3500 V while the capillary was effectively kept at ground. The pressure in the external ion source was maintained at 1×10^{-6} Torr via pumping by an 800 L s^{-1} cryopump (Edwards High Vacuum International, West Sussex, England). After entering the external ion source, the ions were guided to the analyzer region of the mass spectrometer by a series of electrostatic ion optics which were optimized for efficient ion transfer. Pressures in the analyzer region were typically maintained at 2×10^{-9} Torr by additional pumping from two 400 L s^{-1} cryopumps. Immediately before entering the analyzer cell, the ions were given a "sidekick" to minimize any z-axis loss.[154] Once in the cell, the ions were trapped using trapping potentials of +1.0 V and +1.4 V on the two opposed trapping plates.

Inside the analyzer cell, the ions were isolated using an RF notch ejection pulse (see Figure 17 for a typical pulse sequence). Following a 3 s cooling delay to allow for
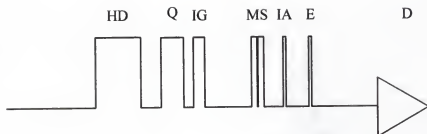
Figure 17. Typical pulse sequence used for the CID studies. HD is the Hexapole Dump, Q is the Quench pulse, IG is the Ion Generation pulse, MS is MS/MS Coarse Selection, IA is the Ion Activation pulse, E is the Excitation pulse, and D is the Detection pulse.

thermalization of the ions, the collision gas was introduced through either a piezoelectric pulsed valve (50 ms pulse) or a leak valve (Varian) to perform CID of the parent ions (cell pressure 1×10^{-7} Torr). A 100 μs RF activation was used to translationally excite the ions, which were then allowed to undergo collisions and fragment during a subsequent 250 ms reaction delay. The resulting reactant and product ions were detected via frequency-chirp excitation. Broadband detection, covering a mass range of 50 to 2500 amu, was utilized in these experiments. During detection, 64 spectra (64k data sets) were normally acquired and signal averaged in order to increase the S/N.

Results

The aim of this project was to determine the gas-phase binding energies between the three common CDs and the twenty essential amino acids, with thoughts of increasing the size of the guest molecule to include peptides and small proteins. The goals of this project were only partially realized. Results for α-CD with tryptophan, proline, and

lysine, and β-CD with tryptophan and histidine are presented below. A reference to the twenty essential amino acids is offered in Table 2 below.

α-CD:Tryptophan

The experimental parameters used to study the [α-CD:Trp]H$^+$ system (as well as the other systems) are summarized in Table 3 (found at the end of the chapter). The tryptophan side chain possesses a nitrogen-containing ring as well as a phenyl ring and is therefore classified as an aromatic amino acid. The cavity diameter of α-CD has been reported to be between 4.7-5.7 Å; therefore, the encapsulation and complexation of the side chain occurs easily by a number of interactions (hydrogen bonding, electrostatic, hydrophobic, and/or van der Waals). Figure 18 shows the isolated complex at m/z 1177. A typical CID mass spectrum depicting the uncomplexed [Trp]H$^+$ (m/z 205) as well as other unidentified fragments is given in Figure 19. Fragmentation of this ion was measured as a function of the ion center-of-mass kinetic energy (an indirect measure of the amount of energy imparted to the ion in the collision). The variable throughout the experiment was the amplitude of the RF excitation pulse, which is to say, the amount of energy imparted in the collision. Attenuation of the RF excitation pulse varied from 11 to 17 dB for the [α-CD:Trp]H$^+$ system (which corresponded to 240.2 to 89.8 V$_{p-p}$ applied the analyzer cell plates). The threshold binding energy was determined by extrapolating the linear portion of the graph to zero (see Figure 20). The threshold binding energy for [α-CD:Trp]H$^+$ was determined to be 1.32 eV.

Table 2. The twenty essential amino acids along with their appropriate symbols and masses.

$$H_2N \longrightarrow CH \longrightarrow COOH$$
$$|$$
$$R$$
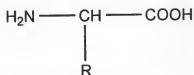
General Amino Acid Structural Unit With Distinctive R Group

Name	R group	Symbols	Monoisotopic Mass	Average Mass
Nonpolar, aliphatic R groups				
Glycine	-H	Gly, G	57.02146	57.0520
Alanine	-CH$_3$	Ala, A	71.03711	71.0788
Proline	-(CH$_2$)$_3$-	Pro, P	97.05276	97.1167
Valine	-CH(CH$_3$)$_2$	Val, V	99.06841	99.1326
Leucine	-CH$_2$CH(CH$_3$)$_2$	Leu, L	113.08406	113.1595
Isoleucine	-CH(CH$_3$)C$_2$H$_5$	Ile, I	113.1595	113.1595
Aromatic R groups				
Phenylalanine	--CH$_2$C$_6$H$_5$	Phe, F	147.06841	147.1766
Tyrosine	-CH$_2$C$_6$H$_4$OH	Tyr, Y	163.06333	163.1760
Tryptophan	-CH$_2$(C$_2$H$_2$N)C$_6$H$_4$	Trp, W	186.07931	186.2133
Polar, uncharged R groups				
Serine	-CH$_2$OH	Ser, S	87.03203	87.0782
Threonine	-CH(CH$_3$)OH	Thr, T	101.04768	101.04768
Cysteine	-CH$_2$SH	Cys, C	103.00919	103.1448
Asparagine	-CH$_2$CONH$_2$	Asn, N	114.04293	114.1039
Glutamine	-(CH$_2$)$_2$CONH$_2$	Gln, Q	128.05858	128.1308
Methionine	-(CH$_2$)$_2$SCH$_3$	Met, M	131.04049	131.1986
Positively charged R groups				
Lysine	-(CH$_2$)$_4$NH$_2$	Lys, K	128.09496	128.1742
Histidine	-CH$_2$(C$_3$H$_3$N$_2$)	His, H	137.05891	137.1412
Arginine	-(CH$_2$)$_3$NH-C(N$_2$H$_3$)	Arg, R	156.10111	156.1876
Negatively charged R groups				
Aspartate	-CH$_2$COOH	Asp, D	115.02694	115.0886
Glutamate	-(CH$_2$)$_2$COOH	Glu, E	129.04259	129.1155

α-CD:Proline

Proline has an aliphatic ring and is, therefore, classified as a nonpolar amino acid. Figure 21 is the mass spectrum of the isolated [α-CD:Pro]H$^+$ at m/z 1088. A typical CID mass spectrum depicting the free protonated proline (m/z 116) as well as the parent ion is presented in Figure 22. Attenuation of the RF excitation pulse used for the [α-CD:Pro]H$^+$ system ranged from 13 to 19 dB (169.7 to 65.2 V$_{p-p}$). Figure 23 highlights the linear portion of the graph which resulted in a threshold binding energy of 1.21 eV when extrapolated to zero.

α-CD:Lysine

The side chain of lysine possesses an amine group and lysine is thus classified as a positively charged amino acid. The isolated parent ion (m/z 1119) can be seen in the mass spectrum shown in Figure 24. Figure 25 is a representative CID mass spectrum of [α-CD:Lys]H$^+$ showing the free protonated lysine (m/z 147) as well as the parent ion. Attenuation of the RF excitation pulse used for [α-CD:Lys]H$^+$ varied from 12 to 30 dB (204.9 to 17.83 V$_{p-p}$). Figure 26 depicts the linear portion of the graph which resulted in a threshold binding energy of 0.71 eV when extrapolated to zero.

β-CD:Tryptophan

The cavity of the β-CD is larger than that of the α-CD; therefore, the encapsulation of the amino acids should be facilitated. The isolated [β-CD:Trp]H$^+$ at m/z 1339 can be seen in the mass spectrum depicted in Figure 27. A typical CID mass spectrum is illustrated in Figure 28. The free protonated tryptophan (m/z 205) can be seen in the expanded region of the spectrum. Attenuation of the RF excitation pulse for

[β-CD:Trp]H$^+$ varied from 11 to 20 dB (240.2 to 57.1 V$_{p-p}$). Figure 29 depicts the linear portion of the graph which resulted in a threshold binding energy of 0.58 eV when extrapolated to zero.

β-CD:Histidine

Histidine is classified as a positively charged amino acid since the side chain contains a ring with two nitrogen atoms. Figure 30 shows the mass spectrum depicting the isolated parent ion at m/z 1290. Attenuation of the RF excitation pulse for [β-CD:His]H$^+$ ranged from 12 to 21 dB (204.9 to 50.7 V$_{p-p}$). A CID mass spectrum showing the free protonated histidine (m/z 156) as well as the parent ion is given in Figure 31. The threshold binding energy was determined to be 0.73 eV from the graph in Figure 32.

Discussion

Unfortunately, a great deal of information cannot be inferred from these data due to the limited number of systems. A comparison can be made between the complexation of tryptophan to α-CD and β-CD. The intermolecular forces that bind the tryptophan to the interior of the CD would presumably be stronger for the α-CD case due to the smaller diameter. With a smaller cavity diameter (closer proximity of atoms), the α-CD would bind more tightly to the tryptophan than the β-CD would. This is reflected in the two threshold binding energies that were measured; 1.32 and 0.58 eV for the α-CD and β-CD systems, respectively. It appears that twice the energy was necessary upon collision to eject the tryptophan from the α-CD cavity than the β-CD cavity.

The threshold binding energy between α-CD and lysine, tryptophan, and proline can be compared since the cavity size in each case remains the same. Given the size of the α-CD cavity the binding strength should be the greatest for tryptophan and the weakest for lysine. Since the side chain of lysine is simply a straight chain (weakest intermolecular forces), the lysine would not be encapsulated as tightly as with the other two amino acids. As for the tryptophan and proline case, they both possess a ring and, therefore, would be of comparable size. However, the tryptophan would extend deeper into the cavity. In addition, the intermolecular forces holding the tryptophan complex together would be stronger due to the increased mass over the proline complex (all other intermolecular forces taken to be equal). The calculated binding energies did, in fact, follow this trend yielding 1.32, 1.21, and 0.71 eV for α-CD with tryptophan, proline, and lysine, respectively.

Table 3. Conditions for studying the various [CD:amino acid]H$^+$ complexes.

	α-CD:Trp	α-CD:Pro	α-CD:Lys	β-CD:Trp	β-CD:His
[CD] (M)	8.20×10^{-4}	8.20×10^{-4}	2.06×10^{-5}	2.06×10^{-5}	2.06×10^{-5}
[amino acid] (M)	3.59×10^{-3}	8.13×10^{-3}	2.33×10^{-3}	5.43×10^{-3}	4.25×10^{-3}
L1 (V)	143.9	82.3	136.6	155.4	142.3
L2 (V)	23.5	26.3	27.9	27.1	18.1
L3 (V)	-3.3	-1.6	-22.8	6.5	25.2
L4 (V)	-48.6	-49.9	-55.3	-34.8	-56.1
L5 (V)	103.8	102.1	106.9	85.9	103.7
capillary temperature (°C)	132	132	132	130	134
needle voltage (V)	3397	3406	3403	3400	3410
flow rate (µl hr^{-1})	60	60	60	60	60
collision gas	Kr	Kr	Kr	Kr	Kr
collision gas pressure (Torr)	$\sim 5.0 \times 10^{-8}$	$\sim 5.0 \times 10^{-8}$	$\sim 5.0 \times 10^{-8}$	$\sim 5.0 \times 10^{-8}$	$\sim 5.0 \times 10^{-8}$
RF amplitude (V$_{P-P}$)	240.2-89.8	169.7-65.2	204.9-17.83	240.2-122.2	204.9-50.7
RF pulse width (µs)	50	50	50	50	50
Binding Energy (threshold, eV)	1.32	1.21	0.71	0.58	0.73
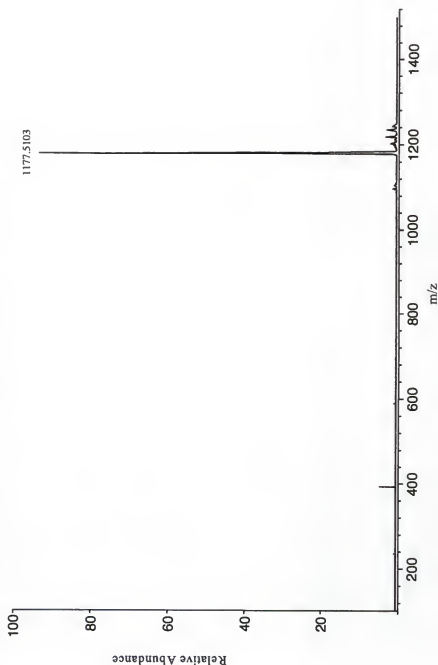
Figure 18. Mass spectrum of the isolated [α-CD:Trp]H$^+$ at m/z 1177. The unlabeled peaks demonstrate the inefficient ejection of unwanted ions during the isolation of the parent ion.
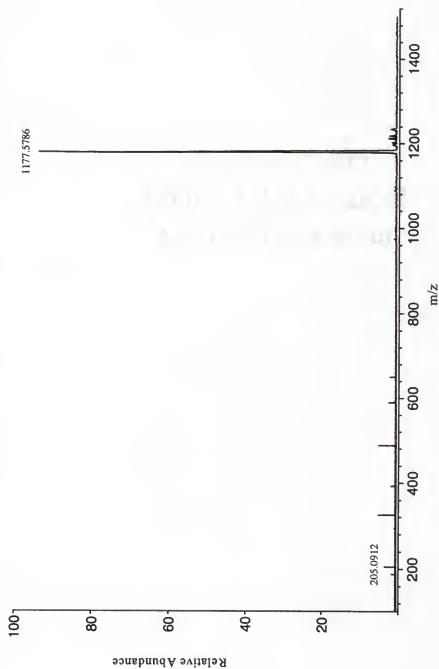
Figure 19. The CID mass spectrum of [α-CD·Trp]H$^+$ showing the free protonated tryptophan at m/z 205.
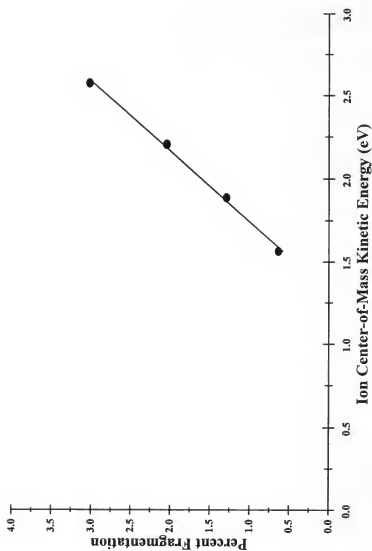
Figure 20. Percent fragmentation versus ion center-of-mass energy for [α-CD:Trp]H$^+$. Extrapolation of this line to zero yields a threshold binding energy of 1.32 eV.
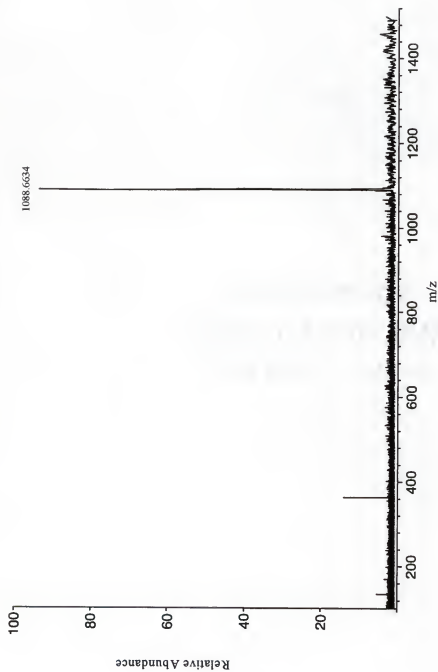
Figure 21. Mass spectrum of the isolated [α-CD:Pro]H⁺ at m/z 1088.
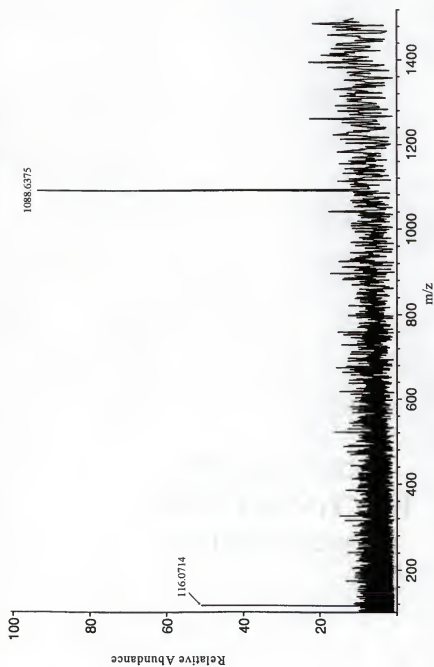
Figure 22. The CID mass spectrum of [α-CD:Pro]H$^+$ showing the free protonated proline at m/z 116.
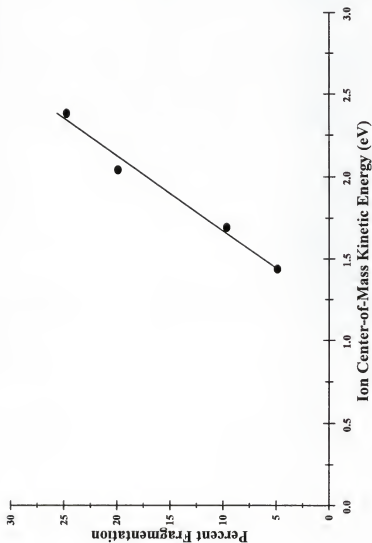
Figure 23. Percent fragmentation versus ion center-of-mass energy for [α-CD:Pro]H$^+$. Extrapolation of this line to zero yields a threshold binding energy of 1.21 eV.
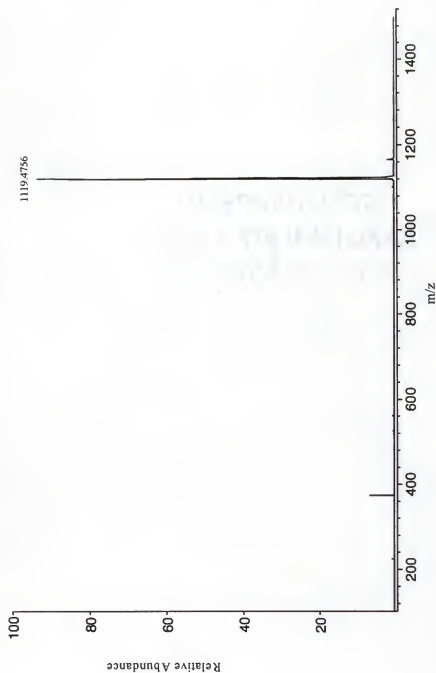
Figure 24. Mass spectrum of the isolated [α-CD:Lys]H⁺ at m/z 1119.
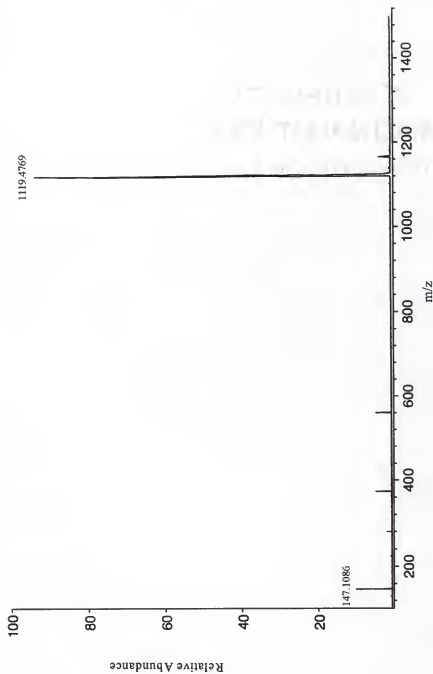
Figure 25. The CID mass spectrum of [α-CD:Lys]H⁺ showing the free protonated lysine at m/z 147.
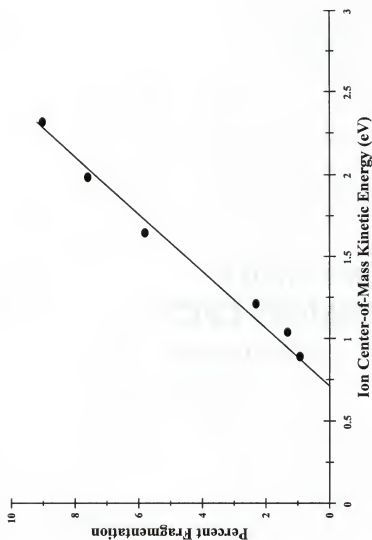
Figure 26. Percent fragmentation versus ion center-of-mass energy for $[\alpha\text{-CD:Lys}]H^+$. Extrapolation of this line to zero yields a threshold binding energy of 0.71 eV.
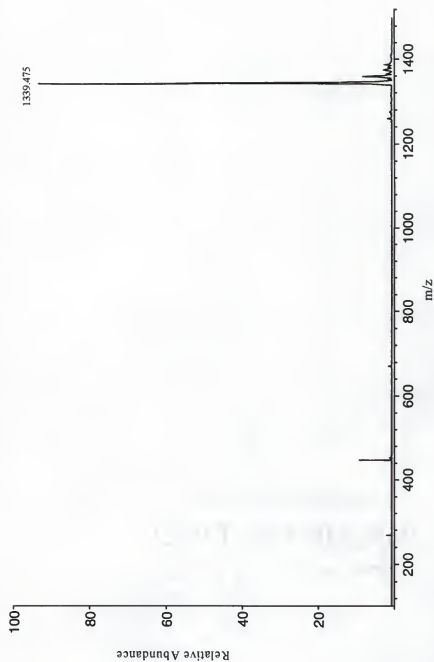
Figure 27. Mass spectrum of the isolated [β-CD:Trp]H$^+$ at m/z 1339.
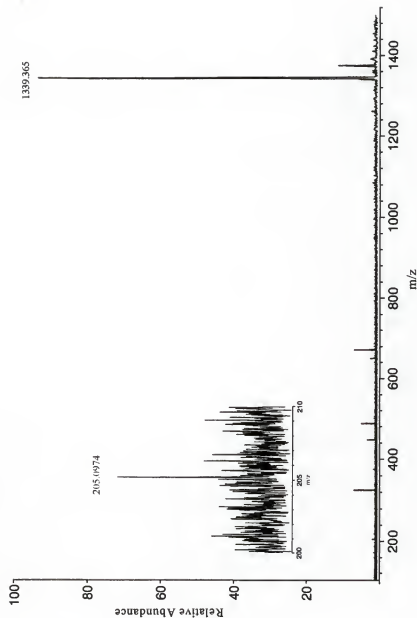
Figure 28. The CID mass spectrum of [β-CD:Trp]H$^+$. The free protonated tryptophan at m/z 147 can be seen in the expanded portion of the spectrum.
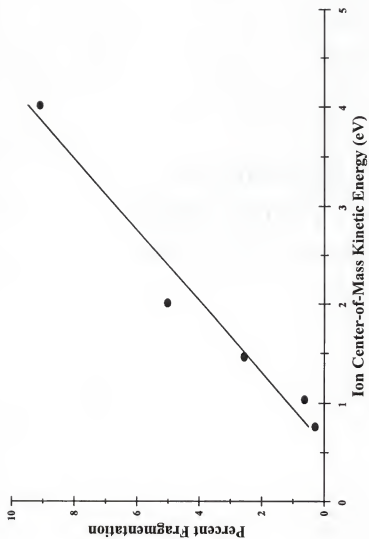
Figure 29. Percent fragmentation versus ion center-of-mass energy for [β-CD:Trp]H$^+$. Extrapolation of this line to zero yields a threshold binding energy of 0.58 eV.
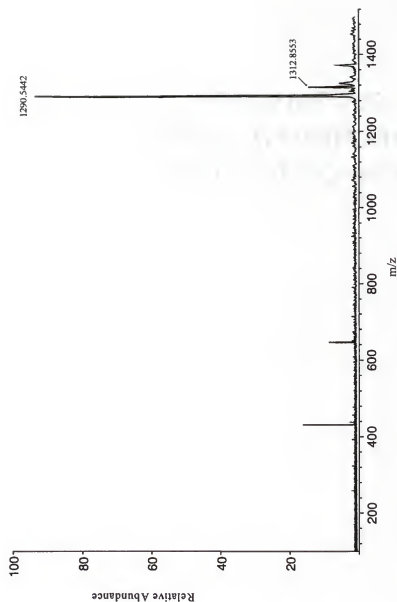
Figure 30. Mass spectrum of the isolated [β-CD:His]H⁺ at m/z 1290.
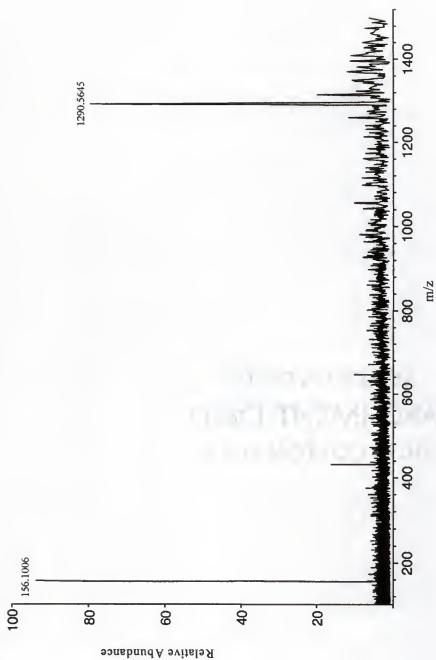
Figure 31. The CID mass spectrum of [β-CD:His]H⁺ showing the free protonated histidine at m/z 156.
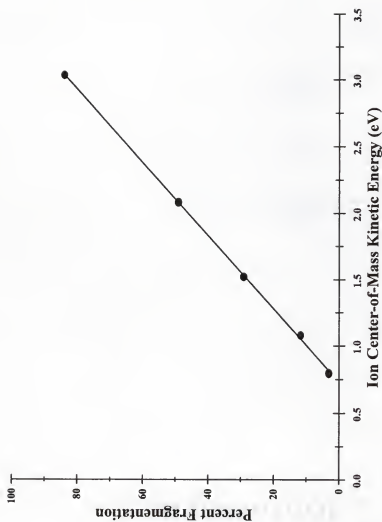
Figure 32. Percent fragmentation versus ion center-of-mass energy for [β-CD:His]H$^+$. Extrapolation of this line to zero yields a threshold binding energy of 0.73 eV.

CHAPTER 3
MOTIVATION FOR INVESTIGATING POLYCYCLIC AROMATIC
HYDROCARBONS OF ASTROPHYSICAL IMPORTANCE

Introduction

The work presented in chapters four and five was undertaken with the purpose of studying the products of photodissociation from a series of polycyclic aromatic hydrocarbon cations that have potential interest within the astrophysical community. The goal was to find laboratory analogues of the species that are possible carriers of the diffuse interstellar bands that have been observed in specific regions of space. An appropriate background discussion will be offered in the present chapter to show the importance of these studies. Following the background discussion, a brief review will provide previous experimental results along with the current direction of our research.

Background

Polycyclic aromatic hydrocarbons (PAHs), more simply known as *polyarenes,* embody an extraordinarily large and diverse class of organic molecules that are generated from fused benzene rings. The major sources of PAHs on this planet are crude oil, coal, and oil shale. The fuels produced from these fossil sources constitute the primary source of energy for the industrial nations of the world, and the petrochemicals produced from these raw materials are the basis of the synthetic fibers and plastics industries. Major considerations of this family of molecule have been their prominent roles as

environmental toxins,[155] exemplified by the discovery in the mid-1930s of the carcin-ogenic properties of benzo[a]pyrene and other polyarenes. This discovery was an important landmark in biomedical science since it was the first indication of disease caused not by a microorganism, but by a relatively simple organic molecule. Since this discovery, researchers have found significant levels of these environmental contaminants in the air we breathe, the food we eat, and the water we drink; most of which can be attributed to the burning of fossil fuels as we have continued to exist as an industrialized nation.

During the past two decades, PAHs have again received a considerable amount of interest, but this time it was the astrophysical community that found PAHs to be intriguing molecules. During this time period, researchers have presented insurmountable evidence that PAHs are also important members of the interstellar medium (ISM), quite possibly being the third most abundant detected molecules behind H_2 and CO.[156] Yet, the likely presence of PAH molecules and ions beyond the earth's atmosphere in space is still somewhat of a novelty for many chemists. Even though they have not been unequiv-ocally identified, aromatic and PAH molecules and ions are now generally accepted by the astrophysical community to be present in interstellar and circumstellar environments. Some have even argued for the presence of nonplanar PAHs and of hollow cages of carbon atoms known as fullerene molecules.

The hypothesis that PAHs are present in interstellar and circumstellar environ-ments already has a substantial historical record.[157-162] Discussions dealing with the presence of PAHs in interstellar environments began with the visionary suggestion,[163] in

1956, that related carbonaceous species are responsible for visible diffuse absorption bands. This fact crystallized with the discovery[164] that some astronomical objects emit a broad infrared emission band which peaks at 3050 cm^{-1} as well as other unique emission features[165,166] which peak in the region between 1610 and 890 cm^{-1}. Astronomical objects which emit these features include regions associated with individual stars such as H-II regions and reflection nebulae as well as interstellar clouds like the IR Cirrus, both in our own and other galaxies.[167-170] Soon after their discovery, these infrared emission features were attributed to infrared fluorescence from molecular-sized emitters excited by the absorption of ultraviolet and visible photons.[171,172] The idea that the fluorescence originated from vibrations of chemical groups attached to aromatic constituents of amorphous carbon particles[173] led to the proposal that individual PAH molecules are responsible for the infrared emission due to their stability against photodissociation and the resemblance of laboratory infrared fluorescence data of such species to the astrophysical spectra.[174-176] PAH molecules have also been proposed as carriers of visible diffuse interstellar bands.[156,177,178] Presently, the PAHs responsible for the infrared features are thought to be more abundant (~17% of the cosmic carbon) than all of the other known gaseous interstellar organic molecules combined.[181]

Current models of interstellar and circumstellar chemistry have emphasized planar PAHs with arrangements of hexagonal rings. These rings are more or less compact ("catacondensed") with the general formula C_{6p}:H_{6p} such as coronene ($C_{24}H_{12}$) or elongated polyacenes with the general formula $C_{4n+2}H_{2n+4}$ such as naphthalene ($C_{10}H_8$), anthracene ($C_{14}H_{10}$), or tetracene ($C_{18}H_{12}$).[157] PAHs with loose arrangements of hexagonal

rings, such as those bound by single carbon-carbon bonds, have largely been neglected. In addition, non-hydrocarbon aromatic molecules have also been excluded. Neutral and positively-charged fused-ring molecules such as pyrene, coronene, and ovaline, either completely or partially hydrogenated, have been invoked to account for both the observed broad IR emission features in nebulae[174-176] and the observed diffuse interstellar absorption bands.[177-179] Recent detection of additional sharp emission features[180] has led to the proposal that much simpler linear fused-ring molecules such as naphthalene, anthracene, and tetracene are responsible for the infrared emission and that benzene may also be present in these environments.[181] For example, anthracene has been suggested as the most abundant of these linear polyacenes in the Orion Ridge.[181]

Diffuse interstellar bands (DIBs) are ubiquitous absorption features in astronomical spectra. They absorb from approximately 4,400 Å into the near infrared. Identifying the carriers of the DIBs has become a classic spectroscopic problem of the 20th century. Since their original discovery in 1922 by Heger,[182] these bands have challenged spectroscopists, astronomers, and physicists, and their origin remains the longest standing unsolved problem in all of spectroscopy.[183] During this time, so many suggestions have been made, experiments carried out, and theories proposed that it would be impossible to review them in this work. The experimental challenge was succinctly stated by Johnson[184] almost thirty years ago, "...one not only has to match 25 diffuse interstellar lines as far as wavelengths are concerned, but also as far as intensity. In addition, the... interstellar line widths vary from 40 Å to 1 Å... and are invariant to 0.1 Å..." Since that time, the number of DIBs has grown to nearly 160 and their relative

intensities have been shown to vary from one line-of-sight to another. In addition, some DIBs seem to associate in loosely connected families.[185-187] Wavelength invariance has been taken to indicate that the carriers cannot reside in or on dust particles. This is because particle size, shape, and composition influence peak position and profile, and it is difficult to imagine that the grains along all lines-of-sight are exactly the same.

The criteria which must be met for a particular material to be considered for acceptance as a DIB carrier are that its visible and near-infrared absorption features match the known DIBs in wavelength, bandwidth, and relative intensities while not possessing additional features that are absent in the interstellar spectra. Of the aforementioned 160 DIBs, a carrier for two has almost certainly been identified; the DIBs at 9577 Å and 9632 Å closely agree with expected spectral features due to the C_{60} fullerene cation.[188] Current theories from leading researchers in the field believe that the carriers are PAH cations or, to account for the discrepancies in peak intensities, mixtures of PAH cations and neutrals.

Since PAHs are believed to be ubiquitous and abundant in the interstellar medium[175,176] and are stable against ultraviolet photodissociation, they are attractive candidates for the DIB carriers. Moreover, a large fraction of the PAHs are expected to be ionized in the interstellar medium,[156,176-178] and thus, absorb lower-energy photons (mainly in the visible and near-infrared regions of the spectrum) than their neutral precursors.[189]

Related Studies

The only available data on PAHs for many years have come from absorption

spectra of neutral and ionized PAHs suspended in perturbing media (solid phase[189-191] or

solution[192]) or from gas-phase photoelectron spectra which do not provide information on

all the possible optical transitions.[193] Allamandola was one of the first investigators to

systematically measure the spectroscopic properties of neutral and ionized PAHs in the

ultraviolet, visible, and near-infrared range (1,800-9,000 Å) under conditions relevant to

astrophysical environments. This was accomplished by studying the isolated species in

the least-perturbing solid medium known, neon matrices at 4.2 K. Neon generally

produces shifts in vibronic positions of only a few tenths of a percent with respect to the

gas phase.[194] Since their first report on naphthalene (the smallest PAH) in 1991, the

Allamandola laboratory has published several articles dealing with matrix-isolated PAH

and PAH cations. But, as expressed by Allamandola, even at 4.2 K in a neon matrix,

there still exist matrix effects that are absent in the interstellar medium. The ideal

situation would be to study these systems in the gas phase where perturbations from a

matrix are absent.

Boissel and co-workers[195] reported the results of a study using a FT-ICR MS with

the Penning trap placed in an ultrahigh vacuum cell attached to a closed cycle helium

cryostat. The temperature of the parts ranged from 12 K to 30 K, ensuring a very low rate

of ion-neutral collisions (confirmed by the long trapping times of up to ten minutes). Ions

were produced by laser ablation of a solid PAH pellet located near one of the trapping

plates. The trapped ions were irradiated by a focused cw xenon arc lamp that had a

computer-controlled mechanical shutter to allow light into the cell. The length of irradiation (in other words the amount of energy imparted to the ions) was varied throughout the experiments. Mass spectra recorded the fragmentation after irradiation of the anthracene, anthracene-d_{10}, and pyrene cations. The photodissociation pathways were found to be the loss of C_2H_2, C_2D_2, and H_2 (or two hydrogen atoms) for the three previously listed ions, respectively.

Two more papers appeared in the literature in late 1997 that pertained to PAHs and astrophysical implications. Ekern and co-workers[196] used FT-ICR MS to study the coronene and naphtho[2,3-a]pyrene cations. Upon irradiation from a xenon arc lamp, each of the two ions was found to dehydrogenate completely to leave the C_{24}^+ bare carbon cluster cation. In the second paper, Wang et al.[197] examined the CID mass spectra of a series of PAH cations using a modified ion trap. Ions of interest were the naphthalene, acenaphthylene, acenaphthene, anthracene, phenanthrene, pyrene, coronene, and the corannulene cation. Mass spectra were recorded after the selected PAH cation was allowed to undergo collisions with argon buffer gas at a pressure of $1\text{-}3 \times 10^{-4}$ Torr. Several different fragment ions were observed and are reported in Table 4.

Ekern et al.[198] extended their earlier study by examining the photostability of a series of twenty-four PAH cations and one fullerene, C_{60}^+. Electron impact and laser desorption were used to generate the ions which were then trapped and mass-analyzed by an FT-ICR mass spectrometer incorporating a 3 T magnet. The trapped ions were subjected to irradiation from a xenon arc lamp and the fragmentation products were recorded. From this series of PAH cations, it was discovered that the observed fragmentation patterns fell into one of four categories: photostable, loss of hydrogen atoms only,

Table 4. Observed fragmentation channels and efficiencies for selected PAH cations using the ion-trap detector. (Reproduced from reference 197)

PAH[a]	[a]Relative abundance of fragment ions							[b]E_f(%)
	$(M-H)^+$	$(M-2H)^+$	$(M-3H)^+$	$(M-4H)^+$	$(M-2C,2H)^+$	$(M-2C,3H)^+$	$(M-2C,4H)^+$	$(M-4C,2H)^+$	
naphthalene	100	95	0	0	10	0	0	1	90
acenaphthylene	100	60	0	0	20	0	0	0	40
acenaphthene	100	30	0	0	5	0	0	0	75
phenanthrene	5	100	0	10	35	15	20	0	75
anthracene	100	65	0	10	50	20	30	0	65
pyrene	40	100	20	60	0	0	0	0	65
coronene	35	100	0	0	25	10	15	0	75
corannulene	40	100	10	100	0	0	0	0	50

[a] The relative uncertainty in the relative abundance is about fifteen percent.
[b] The fragmentation efficiency, E_f, is the fraction of the product ion intensity following CID expressed as a percentage. It is the ratio of the sum of the daughter ion intensities to the total ion intensity of the daughter ions and the undissociated parent ion detected after CID.

loss of hydrogen and carbon atoms, and photodestroyed. Their results are condensed in

Table 5. No real correlation was found to explain why certain PAH cations fragment one

way while a very similar cation will fragment in a different fashion (*e.g.* naphthalene vs.

anthracene).

<div align="center">Current Efforts</div>

Our efforts to study the photodissociation of PAHs of astronomical importance

began where the work of Ekern *et al.*[198] left off. Our initial plans were to continue with

their work by examining wavelength-dependent photodissociation of the same ions. In

the previous work, each of the twenty-four ions was generated, trapped, and irradiated

with the full spectrum from a xenon arc lamp for 500 ms. After the 500 ms irradiation

Table 5. A list of the twenty-four PAHs examined by Ekern *et al.* placed within the appropriate fragmentation category.

Photostable	Loss of H atom(s)	Loss of H and C atom(s)	Photodestroyed
acenaphthylene	fluoranthene	phenanthrene	naphthalene
azulene	pyrene	chrysene	decacyclene
biphenylene	perylene	anthracene	
fullerene, C_{60}	benzo[*ghi*]perylene	diphenylacetylene	
	acenaphthene	benz[*a*]anthracene	
	coronene	benzo[*k*]fluoranthene	
	triphenylene	benzo[*a*]pyrene	
	fluorene	tetracene	
	naphtho[2,3-*a*]pyrene	dibenzanthracene	

period the resulting mass spectrum was recorded. We believed a closer study of the dissociation was warranted for these systems. We generated ions with internal EI and trapped them in an open-ended analyzer cell. The trapped ions were mass analyzed by a FT-ICR mass spectrometer incorporating a 2 T magnet. Several modifications were made, including the design and construction of a much larger cell to allow more light to enter. A computer-controlled mechanical shutter was also built in-house. The source of irradiation was an argon ion laser used to pump a dye laser. After several months of designing, constructing, and troubleshooting, the studies were ready to begin. At first, we did not observe any photodissociation for the PAHs of interest. We then decided to work with a different molecule that would easily dissociate, *p*-bromochlorobenzene. After some success with this system and after becoming familiar with the experimental setup, we switched back to the PAHs. Once again, we had no success. It was decided that we simply were not accessing the appropriate wavelengths for photodissociation with our

setup. Thus, we decided to take a step back, and use the same xenon arc lamp that Ekern *et al.*[198] used. Our thought was to repeat the experiments while using in-line filters so that we could narrow down the appropriate wavelengths in order to purchase the correct laser dyes. While performing the filter studies, I decided to change the experiment slightly after reading the paper published by Boissel and co-workers. Instead of opening the shutter each time for 500 ms, I started to extend this time. The results of this variation were (as Boissel had witnessed) that at longer irradiation times (up to 60 s) the mass spectra drastically changed from what Ekern *et al.*[198] had reported. Since that time, the photodissociation of the PAHs has been studied by varying the length of irradiation from the xenon arc lamp. The next two chapters will report the findings for the fluorene cation as well as the naphthalene, acenaphthylene, and the diphenylacetylene cations.

CHAPTER 4
PHOTODISSOCIATION AND ION-MOLECULE
REACTIONS OF FLUORENE CATIONS

Introduction

Photodissociation and ion-molecule reactions of fluorene cations using Fourier

transform ion cyclotron resonance mass spectrometry are discussed in this chapter. First,

a brief background of relevant theoretical work will be presented. Next, a review of the

experimental setup used to study fluorene will be offered, including photodissociation

studies using a xenon arc lamp and ion-molecule reactions without the lamp. A mention

of plausible structures for some of the products formed from both lamp-on and lamp-off

experiments will be provided. The chapter will end with concluding remarks and a

mention of future experiments that need to be carried out.

Background

Fluorene ($C_{13}H_{10}$, see Figure 33) falls into the category of nonalternant polyarenes.

A nonalternant polyarene is defined as a PAH molecule that comprises one or more rings

that are other than fused six-membered benzenoid rings.[199]

Previous work performed[198] on the fluorene cation revealed that upon irradiation,

up to five hydrogen atoms were lost from the parent ion. Density functional theory

calculations have been carried out at the B3LYP/4-31G level of theory to determine the

most likely positions for the hydrogen atom losses.[200] The results of the calculations
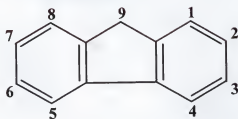
Figure 33. Chemical structure and numbering system of the fluorene molecule (hydrogen atoms have been omitted from the structure).

reveal that the first hydrogen loss is from the sp^3 carbon atom at the number nine position.

The remaining four hydrogen atoms are lost in a sequential order around one of the

aromatic rings. These calculations were employed to determine the energies of the

appropriate cations which might be formed in the photodissociation experiment with no

consideration given to the potential energy barriers that exist on the pathway from one

cation to the next. Figure 34 depicts a flow diagram of the energy pathways leading from

the parent ion at a m/z of 166 to the daughter ion at m/z 161.

Experimental

The underlying principles of FT-ICR MS have been presented earlier. Mass

spectra were acquired on a home-built FT-ICR mass spectrometer incorporating an

IonSpec data station (IonSpec, Corp., Irvine, CA) along with a 2 Tesla superconducting

magnet (depicted in Figure 35). The analyzer cell used throughout these studies was a

cylindrical cell built in-house (see Figures 36-38). Fluorene samples were placed on the

end of a solids probe and introduced directly into the vacuum chamber through a small

gate valve located on the vacuum chamber. The vacuum port which supported the probe
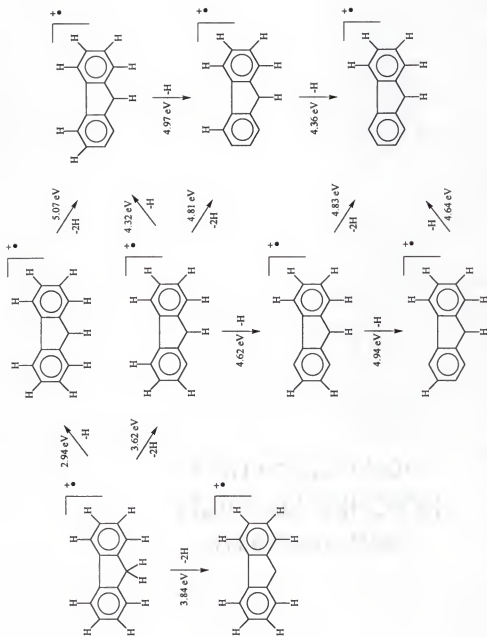
Figure 34. Results of DFT calculations[200] on the fluorene cation outlining the possible fragmentation pathways. The energies were calculated at the B3LYP/4-31G level of theory.

assembly was pumped out by a mechanical pump (Alcatel Vacuum Products, Hingham, MA). Operating pressures in the analyzer cell were typically between $4\text{-}6 \times 10^{-8}$ Torr maintained by a 700 L s^{-1} oil diffusion pump (Alcatel Vacuum Products, Hingham, MA) that was backed by a second mechanical pump.

The analyzer cell was held in position by four stainless steel rods that were connected to a flange at the end of the vacuum chamber; this flange also contained all of the electrical feedthroughs. Due to the weight of the entire cell assembly (rods, rings, EI gun, analyzer cell, connections, etc.), a stainless steel set screw was used to support the free end of the cell assembly. Effort was put forth to ensure that the center of the analyzer cell was located as near as possible to the center of the magnet.

A typical pulse sequence used to generate the mass spectra is depicted in Figure 39. The quench pulse simply emptied the analyzer cell of any unwanted ions that were left over from a previous experiment. In these experiments the quench pulse was set for an unusually long time (500 ms). The extra time was necessary to ensure that the mechanical shutter had enough time to actually come to a closed position. Normally, the quench pulse would be set to ca. 5-10 ms. After the quench pulse there was a short delay period; a similar delay (3 ms) was placed between each event to allow the electronics (particularly the reed relays) to "settle" before the next event. Ions were generated by electron impact ionization of the neutral molecules during the next pulse (usually between 20-50 ms). Electrons were emitted from a heated rhenium filament and accelerated by a potential set by the difference between the ionizing voltage (usually set only a few eV above the ionization potential to minimize the amount of fragmentation from the
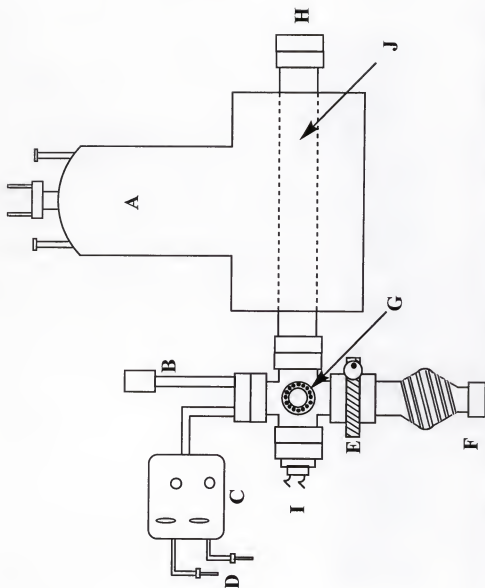
Figure 35. Schematic representation of the 2 T instrument used to study the photodissociation of PAHs. (A) 2 T superconducting magnet, (B) ionization gauge, (C) inlet leak valves, (D) sample tubes, (E) gate valve, (F) oil diffusion pump, (G) solids probe port, (H) irradiation window, (I) connections for the analyzer cell and electron gun, (J) vacuum chamber.

2.7160" i.d.
(2.8145" o.d.)

(end view of the 4 quarter
segments of the analyzer cell)

4.5020"

(a)

2.9790"

(b)

holes drilled and tapped
for 2-56 screws
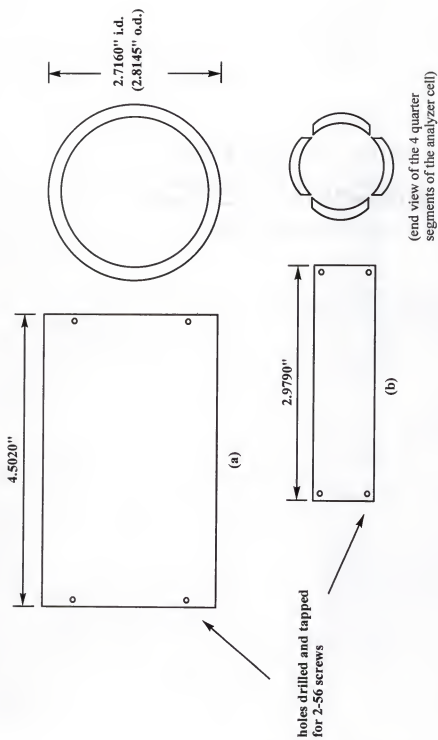
Figure 36. Dimensions of the stainless steel (a) trapping tubes and (b) excitation and detection plates.
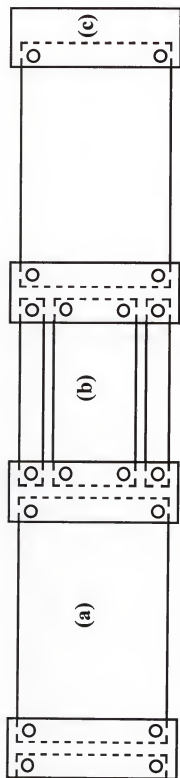
Figure 37. Analyzer cell that was used with the 2 T FT-ICR mass spectrometer to study PAHs. Depicted in the drawing are (a) the two stainless steel trapping tubes, (b) stainless steel tube cut into four equal segments used for the excitation and detection plates, and (c) virgin electrical grade Teflon (TFE) rings used to electrically isolate the different segments of the cell. The overall length of the cell is 3.250". The diameter of the rings is 12.7915" and the diameter of the rings is 3.250".
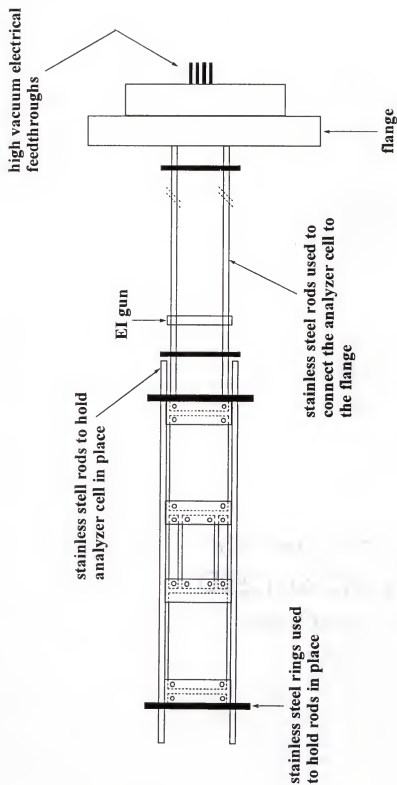
Figure 38. Depiction of the entire analyzer cell assembly used throughout the PAH studies. The analyzer cell was confined between four stainless steel rods that were held together by two stainless steel rings. The entire assembly was attached to a flange that contained the electrical feedthroughs that supplied voltages to the EI gun, trapping plates, and excitation plates.
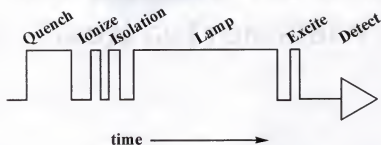
Figure 39. A typical pulse sequence that illustrates the essential steps in obtaining a mass spectrum for the photodissociation studies of the fluorene cation.

ionization process) and the trapping tubes. Even with careful setting of the electron energy, some fragmentation of the parent ion occurred as a result of the EI process; therefore, the next event in the pulse sequence involved ion isolation. This was accomplished by placing an RF sweep over the mass range of unwanted ions or by placing an RF burst directly on an unwanted ion and driving it out of the analyzer cell. Following isolation was the irradiation event, initiated by a computer-generated TTL pulse, that signaled the opening of the mechanical shutter for the specified amount of time. In order to detect the presence of any ions after irradiation, the ions were excited to larger cyclotron orbits to generate the image current that was measured on the detection plates. This image current was amplified, digitized, and stored for processing by the computer.

Studies pertaining to the fluorene cation involved two main themes; detecting photodissociation products and/or detecting ion-molecule products. Photodissociation of the trapped parent ions was accomplished by irradiation supplied by an LX300UV xenon arc lamp (ILC Technology, Sunnyvale, CA) that emitted wavelengths ranging from about

200 to 1100 nm. The lamp was aligned so that the maximum amount of light was transmitted through a window on the end of the vacuum chamber and allowed to enter into the analyzer cell due to the open-ended nature of the cell. The lamp was positioned about a meter from the analyzer cell to minimize effects on it from the fringe field of the magnet; therefore, a focusing lens was employed to narrow the beam into the analyzer cell. A computer-controlled mechanical shutter was used to allow the light into the analyzer cell. This was accomplished by the addition of a *user pulse* within the pulse sequence which has been discussed previously. At long irradiation times, ion-molecule reactions compete with the photodissociation process. Ion-molecule reactions also occur with longer delay times that are placed before the detection event (lamp-off experiments). During both of these types of experiments (long irradiation times and long delay times) larger molecular weight ions began to appear in the mass spectra. These ions will be discussed below.

<div align="center">Results and Discussion</div>

Photodissociation vs. Irradiation Time

As a result of irradiation from the full spectrum of a 300 W xenon arc lamp, the fluorene cation loses up to five hydrogen atoms, depending on the irradiation time. The variable in this set of experiments was the length of the irradiation pulse. The pulse sequence used for these experiments is reproduced in Figure 40. Figures 41 and 42 chart the percent abundance of ions between m/z 166 and 161 as a function of the irradiation time along with typical mass spectra (Figures 43- 45) representing three different irradiation times.

PULSE SEQUENCE	DELAY	WIDTH	OTHER PARAM.
			PAH: Fluorene
			File: DK981210.A01
QUENCH			
E. BEAM	Δ 5.000	500.000	
EJECT 1	Δ 5.000	30.000	
USER A	Δ 5.000	5000.000	m/z 167
DETECT	Δ 5.000	5000.000	Using BNC 15
SIGNAL	Δ 15.000	1.422	m/z 35–750
	Δ .800	16.384	(BB) 2 MHz
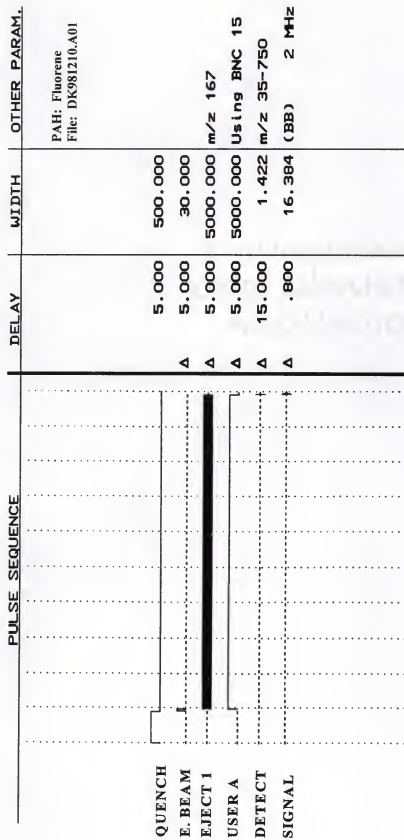
Figure 40. A representative pulse sequence used to study the fragmentation as a function of irradiation time for the fluorene cation. The variable in these experiments was the length of the irradiation pulse (USER A). An ejection pulse was placed on the ion at m/z 167 (which was due to the presence of a carbon-13 atom) in order not to complicate the spectra unnecessarily. This was done in order to ensure that the photodissociation products were derived from the parent ion at m/z 166 and not from the ion at m/z 167.
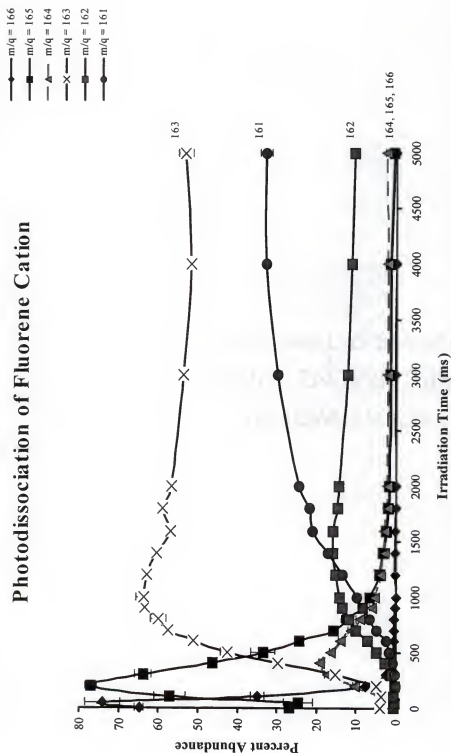
Figure 41. Plot of fragmentation as a function of irradiation time from 0 to 5000 ms for the fluorene cation.
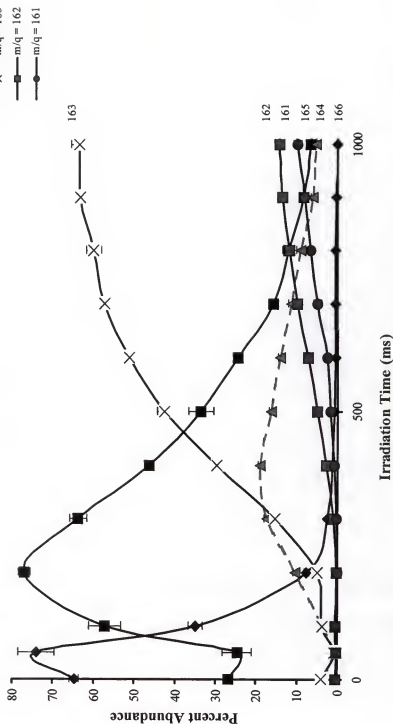
Figure 42. Expanded portion of Figure 41 showing fragmentation as a function of irradiation time from 0 to 1000 ms.

PA#:   Fluorene
File: DK981210.A01
Scans: 20
Scale: 4.5000
Lamp: off
Isolation: none
Ejection: none
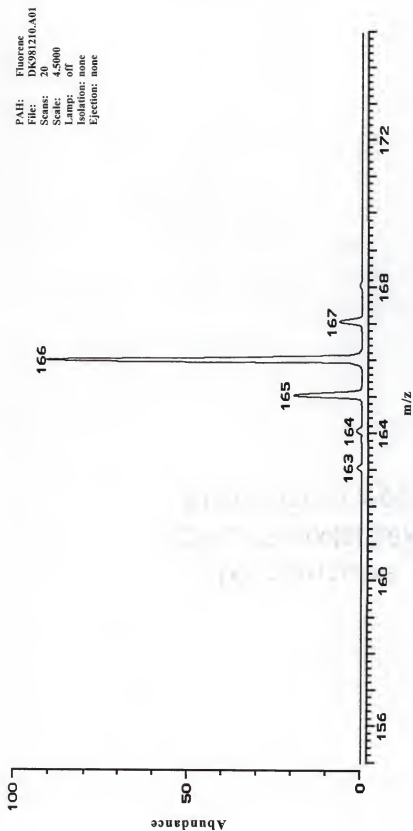
Figure 43. A typical mass spectrum of the fluorene cation. The daughter ions at m/z 163-165 are a result of the EI process.

PAH: Fluorene
File: DK98120.A10
Scans: 20
Scale: 2.2500
Lamp: 200 ms
Isolation: none
Ejection: 167
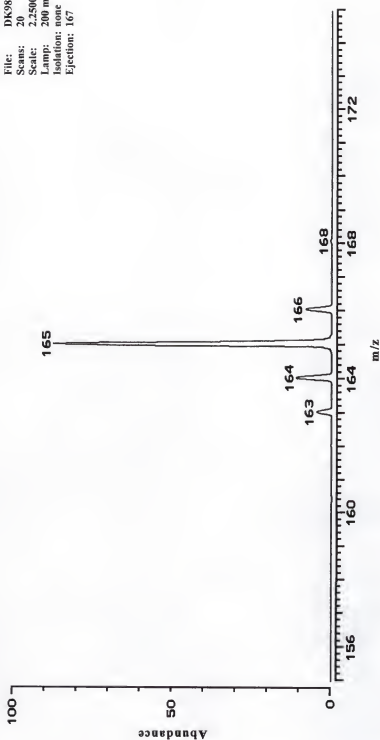
Figure 44. Mass spectrum of the fluorene cation after irradiation of 200 ms. Note that after only 200 ms the daughter ion at m/z 165 now dominates the mass spectrum.

PAH: Fluorene
File: DK981210.A43
Scans: 20
Scale: 7.2500
Lamp: 500 ms
Isolation: none
Ejection: 167
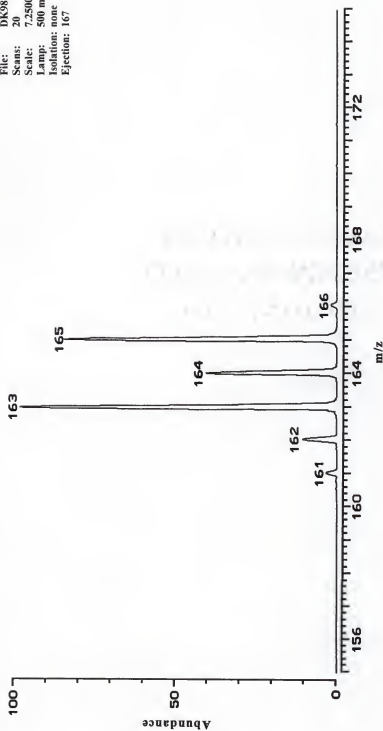
Figure 45. Mass spectrum of the fluorene cation after irradiation for 500 ms. Note that after 500 ms the dominant ion in the spectrum is the daughter ion at m/z 163.

The first daughter ion (m/z 165) is observed in the mass spectrum at t = 0 ms. The ion isolation pulse was found not to be 100% effective at isolating the parent ion at m/z 166, as demonstrated by the abundance of the ion at m/z 165 which resulted from the ionization process. The parent ion had practically disappeared by the time the irradiation approached 300 ms, suggesting that the first hydrogen atom is lost quite easily. Along with this decrease in the parent ion, there was a sharp increase in the abundance of $[M-H]^+$ (where M represents the parent molecule). As mentioned previously, theoretical studies predicted that this hydrogen atom was lost from the sp^3 carbon atom located on the five-membered ring. The abundance of $[M-H]^+$ increased rapidly, reaching a maximum near 200 ms where it began to decrease due to the loss of a second hydrogen atom, resulting in $[M-2H]^+$. After irradiation for 2000 ms, practically all of $[M-H]^+$ was consumed to produce $[M-2H]^+$.

The abundance of $[M-2H]^+$ never reached a level comparable to ions from which it was derived; this indicates that $[M-2H]^+$ is possibly not a stable structure, and therefore, allowed for further dissociation. This ion began to increase after irradiation of about 100 ms and reached a maximum at about 400 ms. This ion, like $[M-H]^+$, is practically gone at long irradiation times. The loss of a third hydrogen atom resulted in the next ion, $[M-3H]^+$, which first appeared after approximately 200 ms of irradiation. The abundance of this ion sharply rose to a maximum at about 1000 ms, where it essentially remained constant out to 5000 ms. A possible explanation as to why the abundance of $[M-3H]^+$ does not rise to a maximum and decrease like the previous daughter ions could be that $[M-3H]^+$ is being formed faster than it is being consumed. There are at least two possible
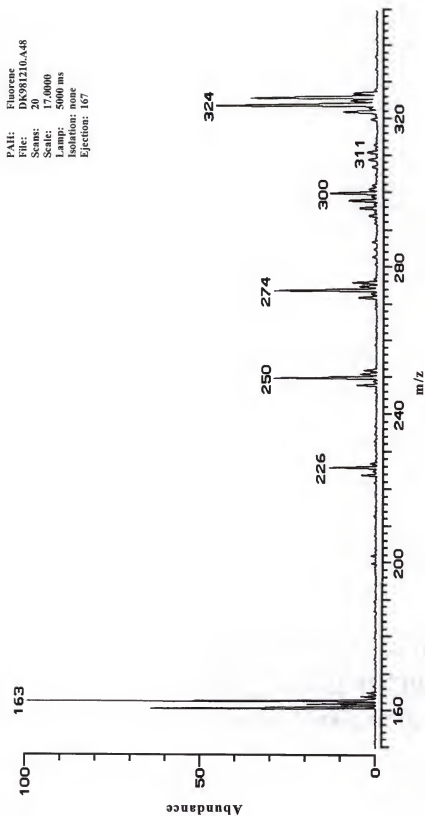
Figure 46. Mass spectrum of the fluorene cation after irradiation for 5000 ms. Note that longer irradiation times lead to new ions as a result of ion-molecule reactions.

mechanisms that could account for the consumption of the $[M-3H]^+$. First, $[M-3H]^+$ could simply continue to dissociate to form the next daughter ion, $[M-4H]^+$. The second possibility is that $[M-3H]^+$ may be involved with ion-molecule reactions that result in ions of larger molecular weight. An example of these ions is shown in Figure 46. These ions are of importance and interest and will be discussed in a later section.

The next ion in the series is $[M-4H]^+$, which slowly began to increase at about 400 ms. The abundance of this ion, like $[M-2H]^+$, increased to a maximum and then decreased as the final daughter ion began to appear. The last ion, $[M-5H]^+$, appeared to behave in a similar fashion to $[M-3H]^+$. It was the last ion to appear (after about 500 ms of irradiation), and its abundance continued to increase out to an irradiation time of 5000 ms. Again, the production of $[M-5H]^+$ (presumably from the $[M-4H]^+$) occurs at a faster rate than its consumption. In this case, the consumption of the $[M-5H]^+$ is solely attributed to ion-molecule reactions, since the loss of more than five hydrogen atoms has not been observed with the experimental design of any of the current or previous experiments[198] involving the fluorene cation.

Atomic vs. Molecular Hydrogen Loss

The question of whether the loss in mass of five amu from the parent ion is by sequential hydrogen atom loss, or possibly, by the loss of a hydrogen molecule was addressed. After ionization of the parent molecule, an isolation pulse was added to isolate the parent ion. The experiment used an irradiation time of 1000 ms which was kept constant. To address the aforementioned question, the experiment was conducted twice. The first experiment simply recorded the mass spectrum of the fluorene ion with

PULSE SEQUENCE		DELAY	WIDTH	OTHER PARAM
				PAH: Fluorene
				File: DK990317.A40
QUENCH	◁	3.000	50.000	
E. BEAM	◁	3.000	300.000	
EJECT 1	◁	3.000	8.098	isol m/z 166
USER A	◁	3.000	1000.000	Using BNC 15
DETECT	◁	3.000	.470	m/z 100-1000
SIGNAL	◁	.800	16.384	(BB) 1MHz
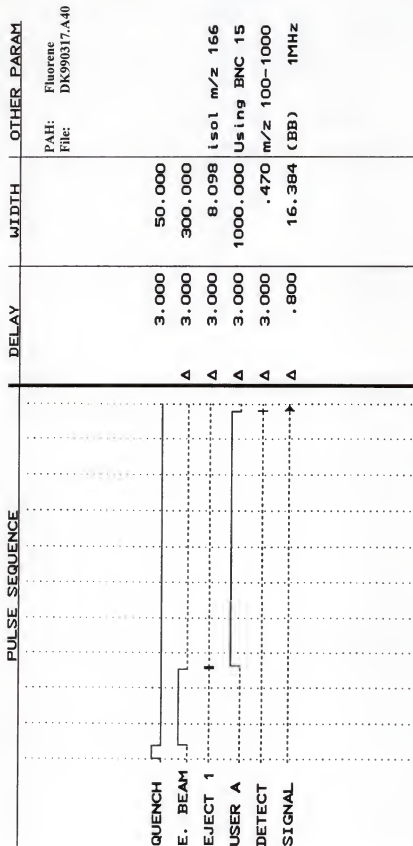
Figure 47. Pulse sequence used to determine if daughter ions of fluorene ions were formed by loss of atomic hydrogens or molecular hydrogens. In this experiment, the isolated parent ion at m/z 166 was exposed to the lamp for 1000 ms.
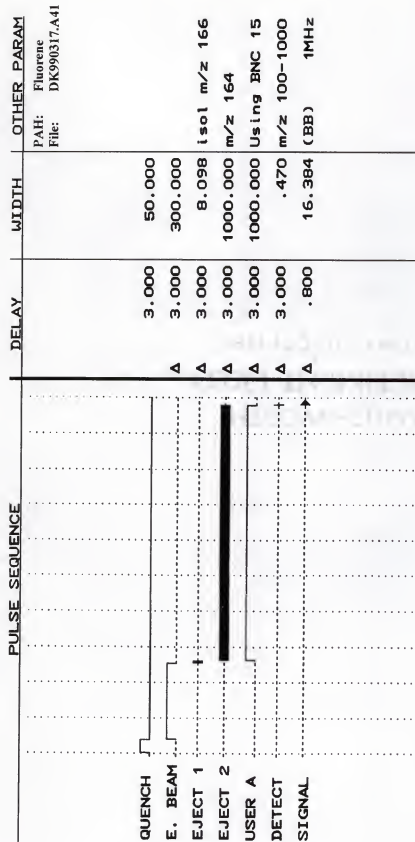
Figure 48. Pulse sequence used to determine if daughter ions of fluorene ions were formed by atomic hydrogen or molecular hydrogen loss. In this experiment, an ejection pulse was placed on the ion at m/z 164 during the irradiation event.

PATI: Fluorene
File: DK990317.A40
Scans: 50
Scale: 14.0000
Lamp: 1000 ms
Isolation: 166
Ejection: off
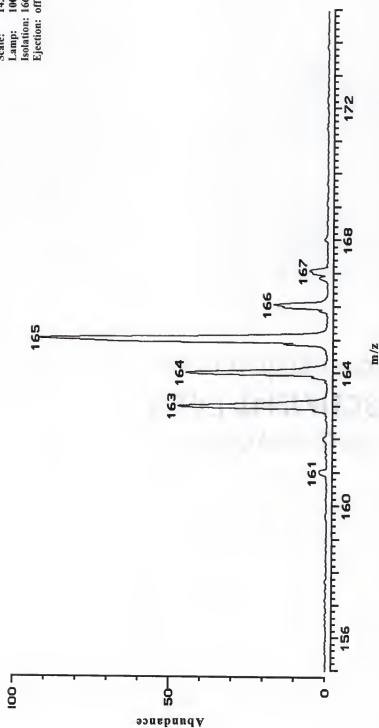
Figure 49. Mass spectrum of the fluorene cation after an irradiation of 1000 ms. In this experiment, the ejection pulse on the ion at m/z 164 was turned off, therefore, all the daughter ions from [M-H]⁻ to [M-5H]⁻ are visible in the spectrum.

PAH: Fluorene
File: DK990317.A41
Scans: 50
Scale: 4.0000
Lamp: 1000 ms
Isolation: 166
Ejection: 164
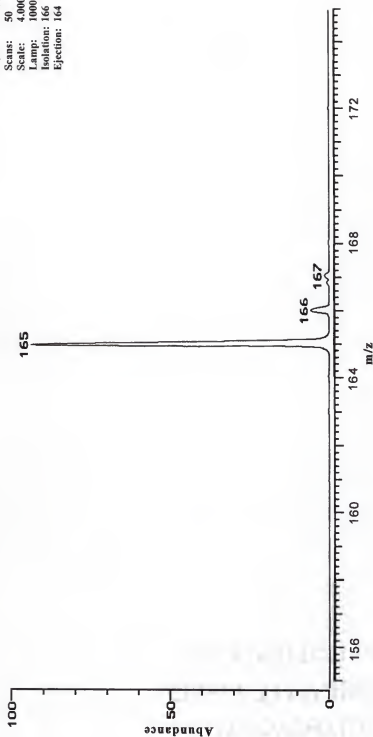
Figure 50. Mass spectrum of the fluorene cation after an irradiation of 1000 ms. In this experiment, the ejection pulse on the ion at m/z 164 was turned on. The absence of the ion at m/z 163 proves that the hydrogens are being lost as atomic hydrogens and not as molecular hydrogens.

an irradiation time of 1000 ms (see Figure 47). In the second experiment, an ejection pulse was introduced into the pulse sequence (see Figure 48). In the first set of experiments (with no ejection pulse), the mass spectrum should be dominated by $[M-3H]^+$ (as well as smaller amounts of $[M-4H]^+$ and $[M-5H]^+$). In the second experiments (with the ejection pulse turned on), $[M-3H]^+$ should be absent from the mass spectrum (as well as $[M-4H]^+$ and $[M-5H]^+$). Figures 49 and 50 are the mass spectra for the experiments with no ejection pulse and the ejection pulse turned on, respectively. From Figure 49, it is clear that $[M-3H]^+$ is the dominant ion at an irradiation time of 1000 ms, along with smaller contributions from the other two ions. On the other hand, Figure 50 shows a very clean mass spectrum with $[M-3H]^+$, $[M-4H]^+$, and $[M-5H]^+$ being absent from the spectrum. This clearly demonstrates that at least for one step of the process, the photo-dissociation of the parent ion is due to the loss of a hydrogen atom and *not* by the loss of a hydrogen molecule. The experiments were repeated with the ejection pulse placed on the ions at m/z 165, 163, and 162 with similar results; hydrogen atoms were lost, not hydrogen molecules.

Ion-Molecule Reactions

As mentioned earlier, at long irradiation times, products of ion-molecule reactions begin to appear and they are ions with larger molecular weights. A typical mass spectrum of this situation is depicted in Figure 51, where the fluorene cation was irradiated for 4000 ms. After irradiation for 4000 ms, the $[M-3H]^+$ is the primary fragment ion remaining, while the parent ion at m/z 166 is essentially gone. However, with the irradiation time extended to much longer times, ion-molecule reactions began to generate

105
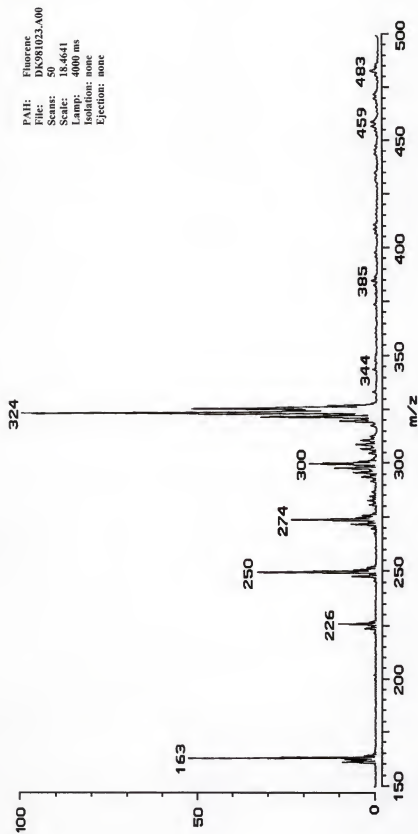
Figure 51. A typical mass spectrum obtained for the fluorene cation after longer irradiation times. This particular experiment had an irradiation time of 4000 ms. At 4000 ms, the parent ion has completely disappeared, leaving [M-3H]⁺ as the dominant fragment ion. Also visible are ions (m/z 226-324) that result from ion-molecule reactions of the neutral parent and fragment ions.
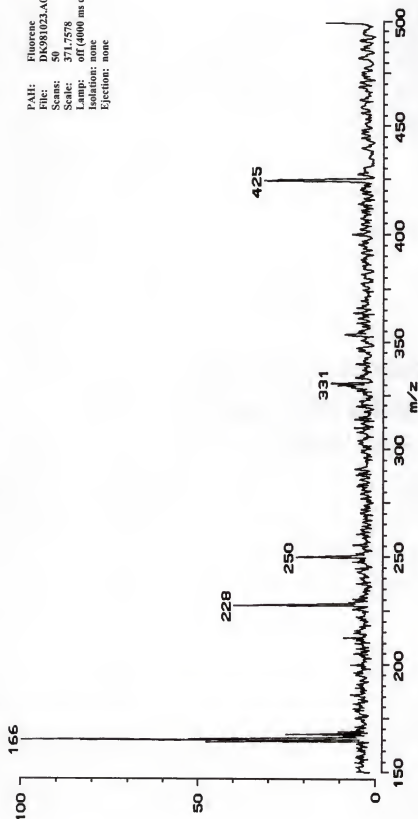
PAH: Fluorene
File: DK981023.A01
Scans: 50
Scale: 371.7578
Lamp: off (4000 ms delay)
Isolation: none
Ejection: none

Figure 52. A mass spectrum with identical conditions as the previous spectrum with one change; the lamp was turned off for this experiment (the 4000 ms was simply a delay time before detection). Note the absence of any ions between m/z 226-324 suggesting that these species are due to ion-molecule reactions initiated by the lamp.

PAH: Fluorene
File: DK98I023.A03
Scans: 50
Scale: 29.3656
Lamp: 500 ms
Isolation: none
Ejection: none
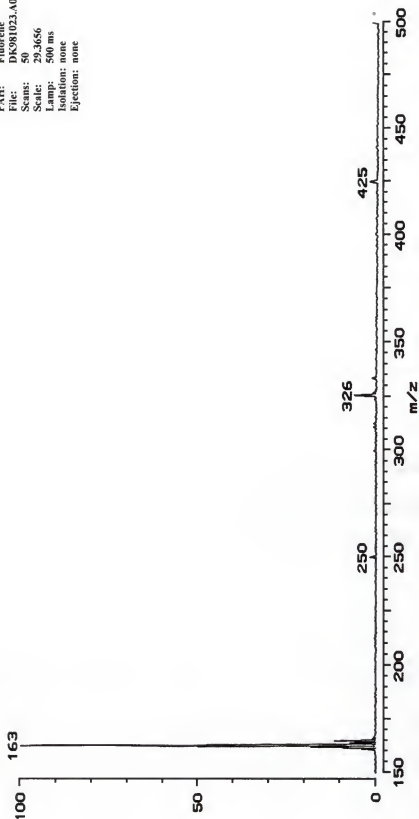
Figure 53. A mass spectrum with identical conditions as in Figure 51 but with an irradiation time of only 500 ms. This spectrum is dominated by $[M-3H]^+$ with only a hint of any ion-molecule reactions occurring. This spectrum thus demonstrates that ion-molecule reactions are not important at shorter irradiation times (< 500 ms).

an ion at m/z 324, which may undergo photodissociation to form smaller fragment ions. If the lamp is turned off for this 4000 ms, the higher molecular weight ions are absent from the mass spectrum, as shown by Figure 52. Here, the conditions are exactly the same except the shutter was not allowed to open. To prove that the ion at m/z 324 did not form at shorter irradiation times, the experiment was again repeated with identical conditions except the irradiation time was only 500 ms, the results are depicted in Figure 53.

A possible explanation for the formation of the ion at m/z 324 comes as the result of an ion-molecule reaction involving the neutral background parent fluorene molecules, which were always present at a pressure of approximately 5×10^{-8} Torr, along with a daughter ion from the fluorene cation. The *bi*-9H-fluoren-9-ylidene (bifluorenylidene) is a likely structure as the initial product from the reaction (see Figure 54a). If this ion is subjected to sufficient irradiation it is possible for a number of hydrogen atoms to be stripped away resulting in the diindeno[1,2,3,4-*defg*;1',2',3',4'-*mnop*]chrysene ion at m/z 324 (see Figure 54b). Bifluorenylidene is a known molecule that has been characterized in a number of ways[201,202] including by x-ray crystallography.[203] The structure in Figure 54b is also a known molecule that has been isolated and studied.[202] The proposed structure for the ion that is formed at m/z 324 is a piece of a "Buckyball" known as a "Buckybowl". If this is truly the structure for this ion, might longer irradiation times (minutes) result in the formation of fullerenes of different sizes? If this were proven true, a new wave of interest in studying PAH cations using FT-ICR MS would prevail with

m/z 328

bi-9H-fluoren-9-ylidene
(bifluorenylidene)

(a)

m/z 324

diindeno[1,2,3,4-*defg*:1',2',3',4'-*mnop*]chrysene
("Buckybowl")

(b)
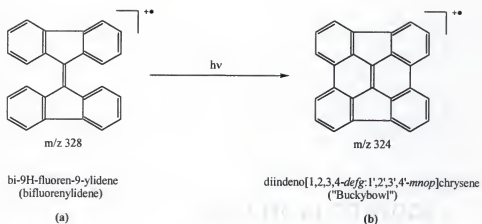
Figure 54. Structure (a) results from a reaction between the neutral fluorene molecules and the fluorene fragment ions. The resulting ion of m/z 328 can further lose hydrogen atoms to form (b) which has a m/z of 324.

collaborations between the astrophysical community and chemists. At the present time,

no effort has been exerted to isolate and photodissociate the ion at m/z 324.

CHAPTER 5
PHOTODISSOCIATION AND ION-MOLECULE REACTIONS OF ACENAPHTHYLENE, DIPHENYLACETYLENE, AND NAPHTHALENE CATIONS

Introduction

The previous chapter concentrated solely on the photodissociation and ion-molecule reactions of the fluorene cation. The present chapter extends these studies to include cations from the three remaining photodissociation groups (as defined by Ekern *et al.*[198]). Specifically, the chapter will be broken down into three sections involving the acenaphthylene cation, the diphenylacetylene cation, and the naphthalene cation. These three cations were photostable, lost hydrogen and carbon atoms, and were photo-destroyed, respectively, after a 500 ms irradiation pulse from a xenon arc lamp.[198] A discussion regarding possible structures for the observed products will be offered along with remarks on future studies.

Acenaphthylene

Acenaphthylene ($C_{12}H_8$, see Figure 55) is a member of the largest category of nonalternant polyarenes which contain one or more five-membered rings. Previous work on the acenaphthylene cation indicated that this cation was photostable after irradiation for 500 ms by a xenon arc lamp.[198] Since the acenaphthylene cation was photostable under the conditions of the earlier experiments, there was no effort to perform any of the

110
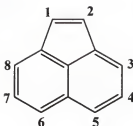
Figure 55. Chemical structure and numbering system for the acenaphthylene molecule (the hydrogen atoms have been omitted from the structure).

theoretical calculations on fragment ion structures as were previously presented for the fluorene cation.

The experimental setup and procedures were the same as previously described so no details will be given. A series of experiments were carried out using very long delay times (with the lamp turned off). This delay was simply placed in the pulse sequence immediately before the detection event. At short delay times, no significant changes in the mass spectrum were detected; the spectrum is dominated by the parent ion at m/z 152 (see Figure 56). But as the delay time increased, a definite change was observed in the mass spectrum. Figure 57 affirms the formation of a new ion near m/z 304 which resulted from an ion-molecule reaction between a neutral acenaphthylene and a acenaphthylene cation. The structure of the 304 ion is most likely that of the known *cis* or *trans* cyclobutane-like dimer[204-209] (see Figure 58). It should be possible to design an experiment to check this assumption. After the long delay time that is necessary to generate the ion, the ion at m/z 304 could be isolated and then subjected to irradiation

PAH: Acenaphthylene
File: k3090625.s13
Scans: 20
Scale: 2.2500
Lamp: Off
Isolation: None
Ejection: None
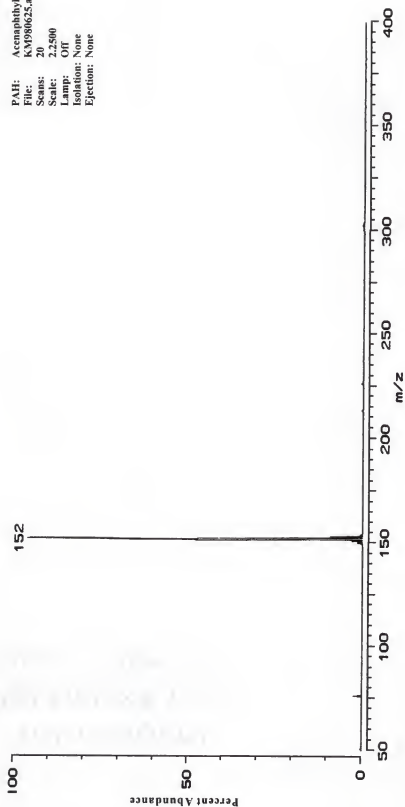
Figure 56. A typical mass spectrum of the acenaphthylene cation after a 500 ms delay was placed before the detection pulse. The spectrum essentially depicts only the parent ion at m/z 152.

113

PAH: Acenaphthylene
File: KM980625.a11
Scans: 20
Scale: 9.0000
Lamp: Off
Isolation: None
Ejection: None
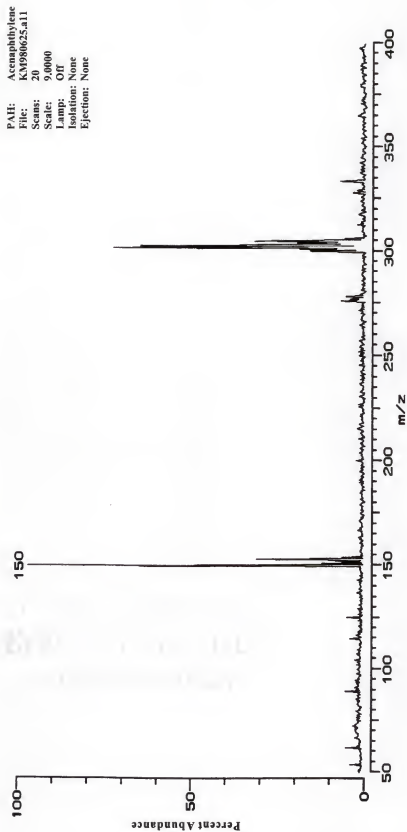
Figure 57. A mass spectrum of the acenaphthylene cation after a 60,000 ms delay time. As a result of the increased delay time, ion-molecule reactions are occurring that generate the ion near m/z 304.
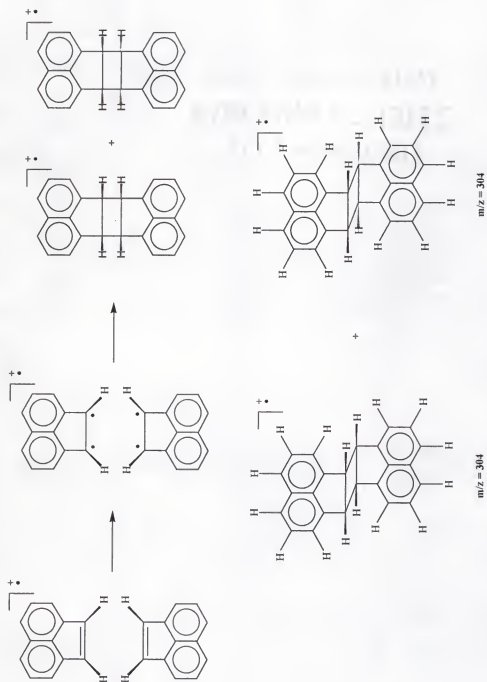
Figure 58. Possible mechanism for the formation of the ion at m/z 304 resulting from an ion-molecule reaction between a neutral acenaphthylene and an acenaphthylene cation.

from the xenon arc lamp. The resulting photodissociation mass spectrum could then be compared to the photodissociation mass spectrum obtained from a purchased or synthesized sample.

The photostability of the acenaphthylene cation that was previously reported was confirmed. However, when longer irradiation times were used, a new ion began to appear in the mass spectrum at m/z 228 (see Figure 59). Since this ion was not observed in the previously discussed experiment (with the lamp off), it is assumed that the ion is a product from the photodissociation of a larger ion; in this case the *cis* or *trans* cyclobutane-like dimer. The assumption is that this ion resulted from the photodissociation of the previously mentioned ion at m/z 304. The ion at m/z 228 arises from a loss of 76 from the dimer-like ion. The proposed scheme for the generation of this ion is depicted in Figure 60. It is possible that this ion undergoes a rapid rearrangement to form the last structure shown in Figure 60. As mentioned before, this proposed structure could be proven if the compound was commercially available.

<div align="center">Diphenylacetylene</div>

Diphenylacetylene is not a true PAH per se, but nonetheless it was a molecule that was previously studied.[198] Figure 61 depicts the structure of the diphenylacetylene molecule. The experimental procedures used to study the diphenylacetylene cation were the same as those used for the previous systems. Diphenylacetylene cations were generated by internal electron impact and both photodissociation (lamp on) and ion-molecule (lamp off) products were mass analyzed using FT-ICR MS.
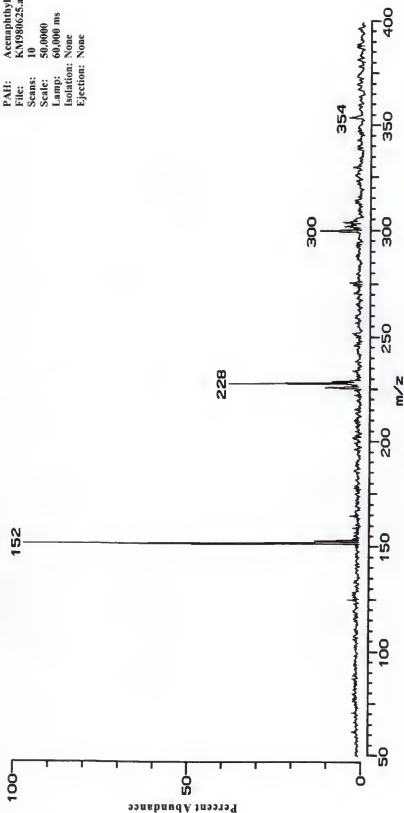
Figure 59. Mass spectrum of the acenaphthylene cation after irradiation for 60,000 ms by a xenon arc lamp. The spectrum depicts the generation of a new ion at m/z 228 which likely forms as a result of the photodissociation of the ion at m/z 304.
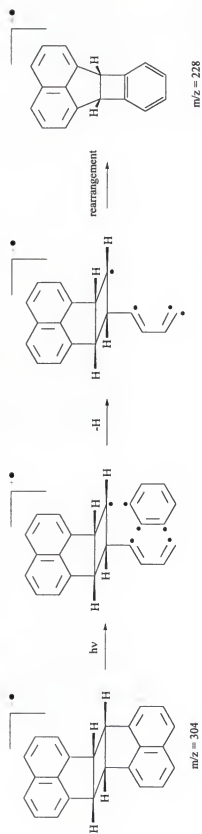
Figure 60. Proposed scheme for the ion observed at m/z 228. This ion is a photodissociation product that is derived from the ion at m/z 304.

Figure 61. Chemical structure of the diphenylacetylene molecule.

The first set of experiments involved placing long delay times before the detection event (lamp off experiments). Figure 62 depicts a characteristic mass spectrum of the diphenyl-acetylene cation after a delay time of only 500 ms. The mass spectrum is dominated by the parent ion at m/z 178 along with traces of ions at m/z 152 and 356. The mass spectrum drastically changed when the delay time was extended. Figure 63 is the mass spectrum following a delay time of 5000 ms. Following this extended delay time, the ion at m/z 356 dominated the mass spectrum. The abundance of this ion increased as a function of delay time as illustrated in Figure 64. Along with the increase in the ion at m/z 356, there was an equal decrease in the parent ion at m/z 178 indicating that the parent ion is directly related to the formation of the ion at m/z 356. In fact, the product ion (m/z 356) most likely results from an ion-molecule reaction occurring between a neutral parent and a parent ion to form a "dimer-like" species. Two possible structures could account for the ion at m/z 356. The first possibility is that a neutral diphenylacetylene and a diphenylacetylene cation simply come together and stack on top of one another (see Figure 65). The second possibility involves the formation of bonds to create a "pinwheel" molecule with a four-membered ring in the center (see Figure 65).

PAII: Diphenylacetylene
File: DK980910.a00
Scans: 20
Scale: 3.7500
Lamp: Off
Isolation: None
Ejection: None
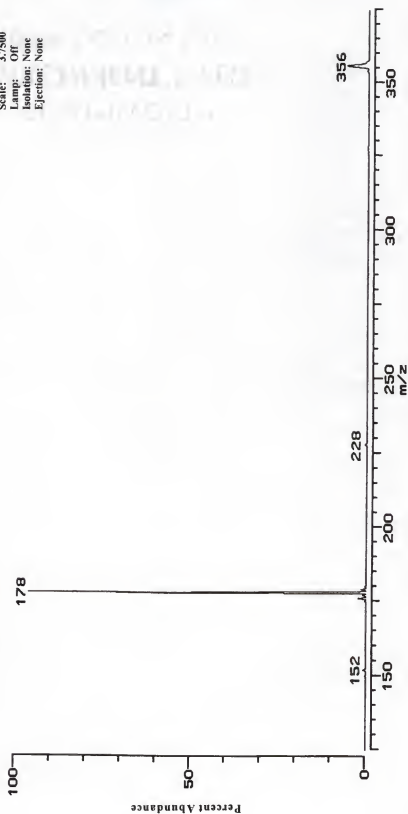
Figure 62. A typical mass spectrum of the diphenylacetylene cation with a 500 ms delay placed before the detection event. At short delay times the mass spectrum is dominated by the parent ion at m/z 178.

120

PAII: Diphenylacetylene
File: DK980910.b22
Scans: 20
Scale: 3.750
Lamp: Off
Isolation: None
Ejection: None

356

228

178

150

m/z

Percent Abundance

100

50

0

150   200   250   300   350
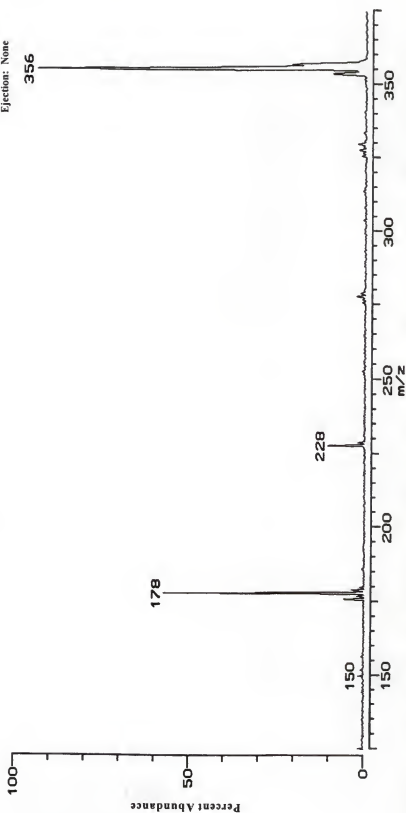
Figure 63. A mass spectrum of the diphenylacetylene cation with a 5000 ms delay placed before the detect event.
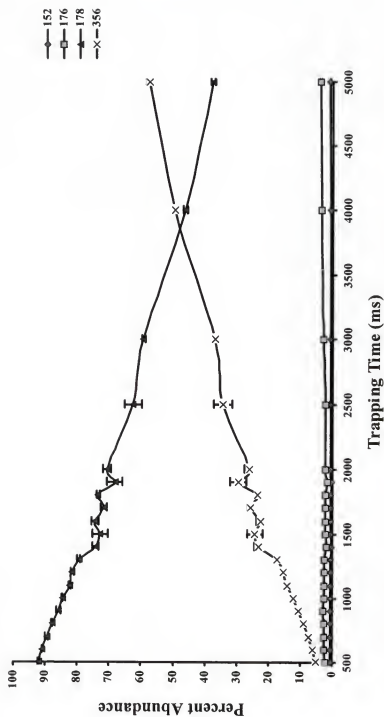
Figure 64. Plot of percent abundance vs. delay time (lamp off) for the diphenylacetylene cation. At longer delay times, ion-molecule reactions resulted in a decrease in the abundance of the parent ion at m/z 178 along with an increase in the abundance of the product ion at m/z 356.
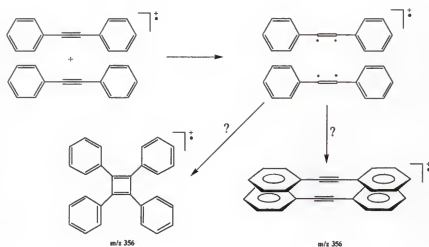
Figure 65. Two possible structures for the ion at m/z 356 that results from an ion-molecule reaction involving a neutral diphenylacetylene and a diphenylacetylene cation.

An experiment was devised to ascertain which of the two structures (assuming one of these two is the correct structure) was the correct one. The plan was to isolate the ion at m/z 356, and then irradiate the ion with the xenon arc lamp. The idea was that if the stacked structure was the correct assumption, it should dissociate relatively easily (after a short irradiation pulse) since this structure is held together through weak interactions. If the pinwheel structure is the true structure, it is assumed that a much longer irradiation pulse would be necessary to dissociate the ion. Also, upon photodissociation, the pinwheel structure would most likely result in several product ions, not just simply reversing back to the parent ion at m/z 178. Unfortunately, these experiments have not been attempted as of this time, but hopefully, they will be implemented in the near future.

The second set of experiments performed on the diphenylacetylene cation analyzed the photodissociation products as a function of irradiation time. With long irradiation times, ion-molecule reactions begin to compete with photodissociation processes. Figure 66 depicts the mass spectrum of the diphenylacetylene cation after irradiation of 500 ms. Comparison of this spectrum with the mass spectrum in Figure 62 shows an increase in the abundance of the ion at m/z 152. The assumption is that the 152 ion is formed from a diphenylacetylene cation that has lost an acetylene group, which would agree with the photodissociation observed by Ekern *et al.*[198] When the irradiation pulse was extended, several new ions began to appear in the mass spectrum (Figure 67). Plausible structures have not been assigned to these new peaks as of yet. They are most likely different photofragments derived from the previously mentioned ion at m/z 356. As previously stated, the ion at m/z 356 is generated after long delay times, but in this case, as soon as the ion is formed it subsequently photodissociated into a number of smaller fragment ions.

From the experiments just described, it is clear that ion-molecule reactions are occurring when long delay times before the detection event are employed. More experiments need to be performed in order to postulate on the structure of the ion at m/z 356. It is also quite evident that long irradiation times generate larger ions that are derived from the ion at m/z 356. Again, more work is needed before any structures can be assigned to these ions.

PAH: Diphenylacetylene
File: D6980910.a03
Scans: 20
Scale: 5.0000
Lamp: 500 ms
Isolation: None
Ejection: None

178

152

Percent Abundance

100

50

0

150   200   250   300   350

m/z
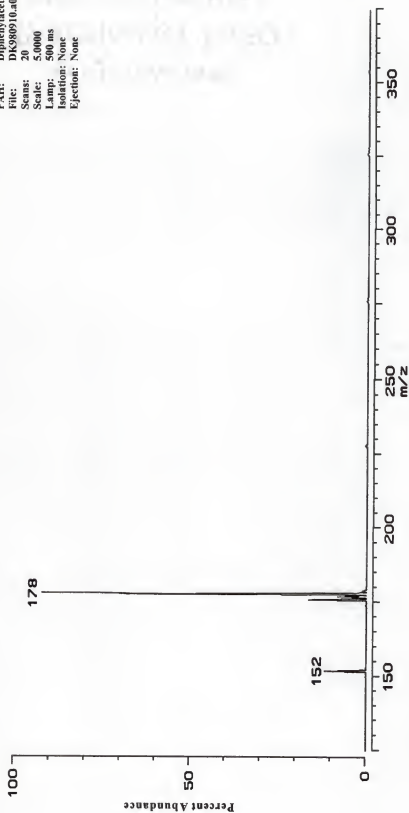
Figure 66. A typical mass spectrum of the diphenylacetylene cation after an irradiation of 500 ms from a xenon arc lamp. The mass spectrum is dominated by the parent ion at m/z 178. The spectrum also depicts a significant abundance of the daughter ion at m/z 152.
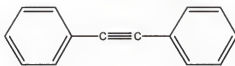
PAH: Diphenylacetylene
File: D6980910.b21
Scans: 20
Scale: 5,000
Lamp: 5000 ms
Isolation: None
Ejection: None
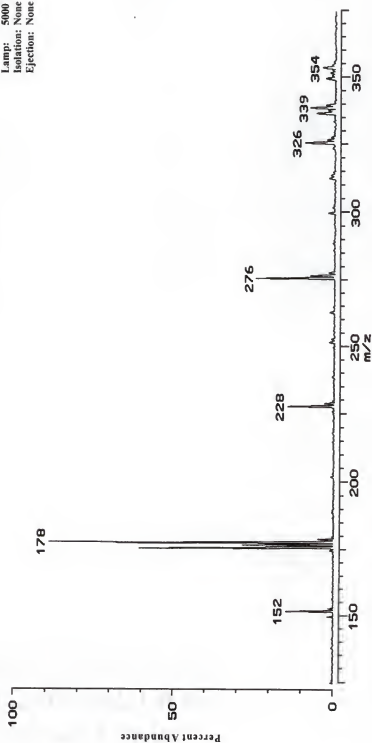
Figure 67. A mass spectrum of the diphenylacetylene cation after an irradiation of 5000 ms. The spectrum depicts the formation of several new peaks which are most likely photofragments resulting from the photodissociation of the ion at m/z 356.

Naphthalene

The last PAH cation to be discussed in this dissertation is that formed from naphthalene. Naphthalene is the simplest member of the nonalternant polyarene group. Previous work on the naphthalene system determined that the naphthalene cation was photodestroyed[198] after only 500 ms of irradiation from a xenon arc lamp. The two proposed routes for the photodestruction of the naphthalene cation are given in Figure 68.

The experimental parameters used for the naphthalene system were, again, the same as with the previous studies. Ion-molecule reactions, resulting from long delay times, were not investigated for the naphthalene cation. Instead, the experiments concentrated on the photodissociation of the cation. Figure 69 depicts a typical mass spectrum of the naphthalene cation after electron ionization. The mass spectrum shows small amounts of dissociation of the cation from the electron impact process itself. A contrasting view is seen in Figure 70 where the naphthalene cation was subjected to an irradiation of 5000 ms from the xenon arc lamp. Again, there is a large abundance of the ions at m/z 102 and 76 (the first two photofragments leading to the total destruction of the ion). But, the spectrum also depicts several new ions, most notably at m/z 202 and 250. Figure 72 offers possible structures for the 202 and 250 ion. The first scheme depicts a neutral naphthalene and a naphthalene cation forming new bonds to generate the benzo-[*ghi*]perylene cation. The second scheme shows the photodissociation of the benzo-[*ghi*]perylene cation followed by a rearrangement resulting in the formation of the fluoranthene cation. Both of these structures are reasonable and should be relatively straightforward to prove.

Figure 68. Two possible routes for naphthalene cation photodestruction. (Taken from reference 198)

A set of experiments were devised and attempted that would hopefully elucidate the structures of the ions at m/z 202 and 250. Benzo[*ghi*]perylene and fluoranthene are two systems that were previously studied and are readily at hand. The idea was to fashion an experiment where the naphthalene cation would be irradiated for 5000 ms, then the ion of choice (m/z 202 or 250) would be isolated using a simple isolation pulse, and finally the selected ion would be subjected to another irradiation pulse lasting 500 ms (to match the conditions used by Ekern *et al.*[198]). Ultimately, the resulting mass spectrum would be compared to the previous work for a match of photodissociation products (loss of

PAH: Naphthalene
File: DK990525.A00
Scans: 100
Scale: 1.6074
Lamp: Off
Isolation: None
Ejection: None
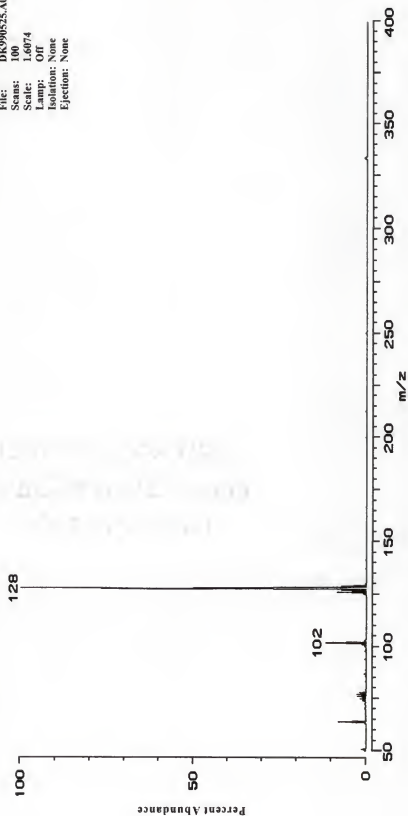
Figure 69. A typical mass spectrum of the naphthalene cation. The spectrum illustrates the tendency of the naphthalene cation to dissociate completely. The ions at m/z 102 and 76 result from the EI process itself.
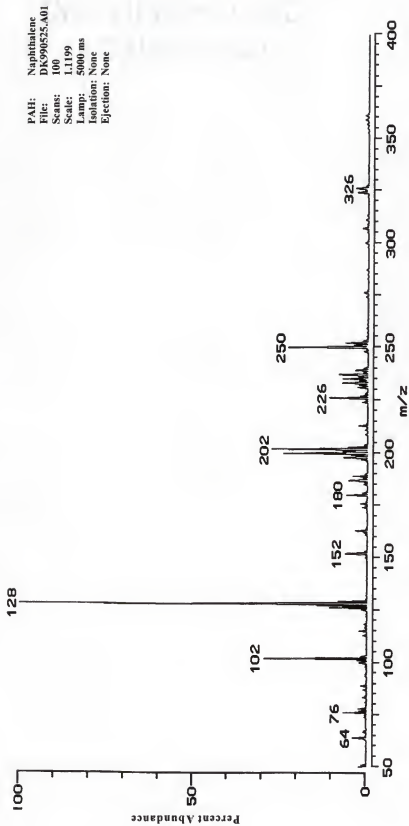
Figure 70. A mass spectrum of the naphthalene cation after an irradiation pulse of 5000 ms. Note the formation of several new ions at masses above 128.
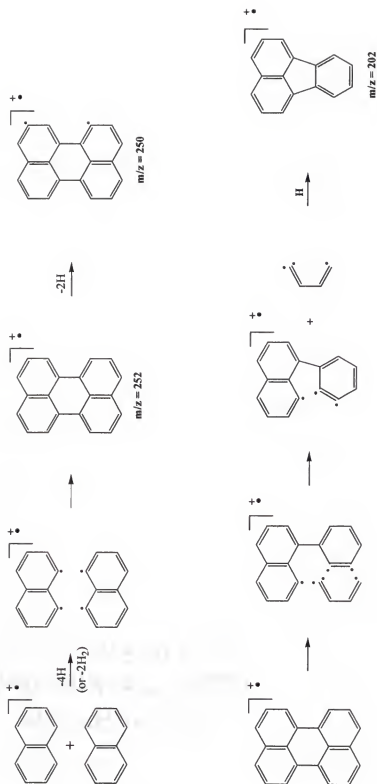
Figure 71. Possible structures for the ions observed at m/z 202 and 250 resulting from irradiation of the naphthalene cation.

hydrogen atoms only for both cations). These experiments were attempted several times with little success. The results were encouraging enough to continue once a few technical problems were overcome. At first, attempts to open the shutter twice within the same pulse sequence did not work. After a little assistance from the electronics shop, this problem was defeated. The next major hurdle is to decrease the length of the irradiation pulse in order to keep as many ions in the analyzer cell as possible, since the longer the amount of time before detection of the ions, the more the ion population decreases. But at the same time, the irradiation pulse has to be long enough to provide an adequate number of ions in order to produce a mass spectrum. It is this author's belief that the above mentioned experiments will be successfully completed.

A very brief remark pertaining to the output of the lamp and the proposed dissociation mechanisms (for example, Figure 68) is given below. The naphthalene cation has several very strong absorption features in the uv region (308 nm for example). The output from the LX300UV lamp is between 200-1000 nm. A quick calculation of the amount of energy needed to rupture the naphthalene cation (as shown in Figure 68) shows that roughly 388 KJ mol^{-1} is required to break the indicated bonds in the proposed mechanisms. The output from the lamp provides several eV of energy (perhaps three or four eV of energy) per photon. It is reasonable to suggest that these ions can absorb two or more photons (especially considering the amount of time they are trapped in the analyzer cell) and therefore acquire more than enough energy to fragment in the manner as proposed in this dissertation. More detailed experiments will, of course, be necessary in the future to ascertain the validity of such claims.

CHAPTER 6
CONCLUDING REMARKS

<u>Binding Energies for CD:Amino Acid Complexes</u>

As mentioned earlier, a great deal of information cannot be inferred from these data due to the limited number of systems. For this reason, there are limited conclusions that can be drawn from the available data. Threshold binding energies of 1.32 and 0.58 eV were determined for the complexation of tryptophan to α-CD and β-CD, respectively. Without further examination of these two systems, the absolute numbers may not be accurate, but the relative numbers do seem to be believable. Since the cavity of the α-CD is the smaller of the two systems, it makes sense that this host would bind more tightly to its guest than the β-CD host would bind to the same guest.

The second conclusion that can be inferred from these data pertains to the threshold binding energy determined for α-CD incorporating a lysine, tryptophan, or proline guest, since the cavity size in each case remains the same. Threshold binding energies of 1.32, 1.21, and 0.71 eV were determined for the α-CD binding with tryptophan, proline, and lysine guests, respectively. Again, the relative numbers are reasonable for this series. The binding strength should be the greatest for tryptophan and the weakest for lysine (side chain is a simple straight chain and would posses the weakest intermolecular forces). As for the tryptophan and proline case, they both possess a ring

132

but the tryptophan would extend deeper into the cavity. In addition, the intermolecular forces holding the tryptophan complex together would be stronger due to the increased mass over the proline complex (all other intermolecular forces taken to be equal).

Much more work can and should be done with these systems in the near future in order to draw better conclusions. Similar work in other laboratories is underway to study the binding of small peptides and proteins to substituted CDs (more water soluble). The CID experiments performed here were not terribly successful for a number of reasons. Most of the work was performed using argon as the collision gas. Only at the end of the project did krypton gas become available. Work in the future could reasonably benefit from an even heavier (but more expensive) gas such as xenon. Many of the leading scientists in this field agree that xenon gas is the best choice for a collision gas. A different method for measuring binding energies in the gas-phase may be beneficial to this project. Due to the size of the CDs (many degrees of freedom), the binding energies may be obtained more easily using a relatively new technique known as BIRD (Blackbody Infrared Radiation Dissociation). Basically, the complexes are trapped in the analyzer cell and allowed to dissociate by absorbing photons that are emitted from the heating of the entire analyzer cell. An initial design incorporating a heated tube to slide over the analyzer cell has been fabricated and tested with little success. Hopefully, this project will continue, but that will be left up to a future student to decide.

Fluorene

The fluorene cation has received more attention than any of the other PAH cations presented in this work. The most obvious observation that can be made from the

presented data, is that the processes that are occurring are very complicated. What complicates the studies is that the lamp is driving the parent ion at m/z 166 down to daughter ions at m/z 165, 164, 163, 162, and 161. If long delay times are used (no lamp) each of these ions is capable of undergoing an ion-molecule reaction with a neutral parent to generate an ion between m/z 331-327. But, when the lamp is used, each of these ions (m/z 331-327) can then fragment, resulting in smaller ions.

From the experiments that measured the photodissociation as a function of irradiation time, one can monitor the increase and decrease in the abundance of the daughter ions at m/z 165, 164, and 162. The abundance of the daughter ions at m/z 163 and 161 did not decrease with increasing irradiation time. The idea here is that these two ions are forming faster than they are being consumed (presumably through ion-molecule reactions). The loss in mass of five amu from the parent ion was also shown to occur by sequential hydrogen atom loss and not by the loss of hydrogen molecules. Experiments utilizing long delay times were presented and demonstrated the formation of new ions that resulted from ion-molecule reactions. These ions were subsequently photodissociated after the application of long irradiation times. A possible structure for the ion at m/z 324 was presented, but more experiments need to be conducted in order to prove (or disprove) the validity of this structure. With the completion of these experiments, I hope there is a little better understanding of the photodissociation processes as well as ion-molecule reactions that are occurring with fluorene cation.

Acenaphthylene

The acenaphthylene cation was photostable after irradiation for 500 ms (as was previously determined[198]). But, with long delay times, ion-molecule reactions did occur that generated an ion at m/z 304. The structure of this ion is most likely that of the *cis* or *trans* cyclobutane-like dimer.[204-209] Irradiation of this ions resulted in the formation of an ion at m/z 228. A proposed structure for this ion (after a rearrangement) was given. A new set of experiments will need to be conducted to prove the validity of this structure.

Diphenylacetylene

Ion-molecule reactions were also observed at long delay times for the diphenylacetylene cation as evident by the formation of a new ion at m/z 356. Two structures were proposed for this ion, along with a relatively straightforward experiment that should be able to determine which structure is the correct one. Irradiation of the parent ion (m/z 178) produced an ion at m/z 152 which is assumed to be the loss of an acetylene group. This observation is in agreement with Ekern *et al.*[198] Longer irradiation times resulted in the generation of several new ions ranging from m/z 276-354. To date, no structures have been proposed for any of these ions.

Naphthalene

There were no lamp off (long delay times) experiments performed on the naphthalene cation. After short irradiation times, the naphthalene cation was found to be photodestroyed (as was previously reported[198]). But when the irradiation time was extended, the mass spectrum depicted the formation of several new ions. Two of the more abundant ions were observed at m/z 202 and 250. Structures were proposed for

both of these ions. Again, a set of experiments were described that should justify the proposed structures.

As has been mentioned previously, much more work needs to be carried out on the four cations described in this thesis. In addition to these cations, there are still the remaining twenty from the previous study[198] that can be examined. It is with deep regret that this author got involved with this project so late in his career. The amount of work that is possible within this area is massive and should keep several students busy for the next few years. Lamp off (ion-molecule reactions) and lamp on (photodissociation) experiments could be performed on hundreds of PAH cations. Eventually, after significant new information has been retrieved for these systems, one could go back to the original starting point of this project, which was wavelength-dependent studies using the argon ion laser. The Eyler laboratory is equipped with a Nd:YAG dye-pumped laser and has access to an argon ion laser. The possibilities are endless. Along with the available equipment (lasers and three FT-ICR mass spectrometers), the Eyler laboratory has just upgraded the data station on the 2 T instrument. The instrument is now controlled by the MIDAS data station which should allow for more sophisticated pulse sequences which include much improved trapping, isolation, and ejection of ions. With the capability of designing more sophisticated pulse sequences, many of the described experiments that could prove proposed structures, should be possible.

LITERATURE CITED

1) Pardue, H. L. (Special Issue: Fourier-Transform Mass Spectrometry: Fundamental Aspects and Analytical Applications.) *Anal. Chim. Acta* **1985**, *178*, 158 pp.

2) Comisarow, M. B.; Nibbering, N. M. M., Eds.; (Special Issue: Fourier Transform Ion Cyclotron Resonance Mass Spectrometry) *Int. J. Mass Spectrom. Ion Processes* **1986**, *72*, 222 pp.

3) Wilkins, C. L. (Special Issue: Fourier Transform Mass Spectrometry) *Trends in Anal. Chem.* **1994**, *13*, pp 223-251.

4) Marshall, A. G. (Special Issue: Fourier Transform Ion Cyclotron Resonance Mass Spectrometry*) Int. J. Mass Spectrom. Ion Processes* **1996**, *157/158*, 407 pp.

5) Buchanan, M. V., Ed.; *Fourier Transform Mass Spectrometry: Evolution, Innovation, and Applications, ACS Symp. Series, Vol. 359*; American Chemical Society: Washington, DC, 1987.

6) Marshall, A. G.; Verdun, F. R. *Fourier Transforms in NMR, Optical, and Mass Spectrometry: A User's Handbook*; Elsevier: Amsterdam, 1990.

7) Asamoto, B., Ed.; *FT-ICR/MS: Analytical Applications of Fourier Transform Ion Cyclotron Resonance Mass Spectrometry*; VCH: New York, 1991.

8) Marshall, A. G.; Hendrickson, C. L.; Jackson, G. S. *Mass Spectrom. Rev.* **1998**, *17*, 1-35 and references cited therein.

9) Lawrence, E. O.; Edlefsen, N. E. *Science* **1930**, *72*, 376-377.

10) Lawrence, E. O.; Livingston, M. S. *Phys. Rev.* **1932**, *40*, 19-35.

11) Hipple, J. A.; Sommer, H.; Thomas, H. A. *Phys. Rev.* **1949**, *76*, 1877-1878.

12) Sommer, H.; Thomas, H. A. *Phys. Rev.* **1950**, *78*, 806.

13) Sommer, H.; Thomas, H. A.; Hipple, J. A. *Phys. Rev.* **1951**, *82*, 697-702.

14)   Llewellyn, P. M. *U. S. Patent* 3,505,517, **1970**.

15)   McIver, R. T., Jr. *Rev. Sci. Instrum.* **1970**, *41*, 555-558.

16)   Comisarow, M. B.; Marshall, A. G. *Chem. Phys. Lett.* **1974**, *25*, 282-283.

17)   Comisarow, M. B.; Marshall, A. G. *Chem. Phys. Lett.* **1974**, *26*, 489-490.

18)   Comisarow, M. B.; Marshall, A. G. *J. Chem. Phys.* **1975**, *62*, 293-295.

19)   Guan, S.; Marshall, A. G. *Int. J. Mass Spectrom. Ion Processes* **1995**, *146/147*, 261-296.

20)   Wineland, D. J. *Science* **1984**, *226*, 395-396.

21)   Schweikhard, L. *Rapid Commun. Mass Spectrom.* **1994**, *8*, 10-13.

22)   Dempster, J. A. *Phys. Rev.* **1918**, *11*, 316-325.

23)   Munson, M. S. B.; Field, F. H. *J. Am. Chem. Soc.* **1966**, *88*, 2621-2630.

24)   Honig, R. E.; Woolston, J. R. *Appl. Phys. Lett.* **1963**, *2*, 138-139.

25)   Yang, L.-C.; Wilkins, C. L. *Org. Mass Spectrom.* **1989**, *24*, 409-414.

26)   Brown, R. S.; Wilkins, C. L. *Anal. Chem.* **1986**, *58*, 3196-3199.

27)   Nuwaysir, L. M.; Wilkins, C. L. *Anal. Chem.* **1988**, *60*, 279-282.

28)   Torgerson, D. F.; Showronski, R. P.; Macfarlane, R. D. *Biochem. Biophys. Res. Commun.* **1974**, *60*, 616-621.

29)   Jonsson, G. P.; Hedin, A. B.; Hakansson, P. L.; Sundqvist, B. U. M.; Säve, B. G. S.; Nielsen, P. F.; Roepstorff, P.; Johansson, K.-E.; Kamensky, I.; Lindberg, M. S. L. *Anal. Chem.* **1986**, *58*, 1084-1087.

30)   Dole, M.; Mack, L. L.; Hines, R. L.; Mobley, R. C.; Ferguson, L. D.; Alice, M. B. *J. Chem. Phys.* **1968**, *49*, 2240-2249.

31)   Dole, M.; Cox, H. L., Jr.; Giemiec, J. *Adv. Chem. Ser.* **1973**, *125*, 73-84.

32)   Dole, M.; Gupta, C. V.; Mack, L. L.; Nakamae, K. *Polymer Preprints* **1977**, *18*, 188-193.

33)   Yamashita, M.; Fenn, J. B. *J. Phys. Chem.* **1984**, *88*, 4451-4459.

34)   Alexandrov, M. L.; Gall, L. N.; Krasnov, V. I.; Nikolaev, V. A.; Pavlenko, V. A.; Shkurov, V. A. *Int. J. Mass Spectrom. Ion Processes* **1983**, *54*, 231-235.

35)   Barber, M.; Bordoli, R. S.; Sedgwick, R. D.; Tyler, A. N. *J. Chem. Soc., Chem. Commun.* **1981**, *7*, 325-327.

36)   Benninghoven, A. In *Ion Formation from Organic Solids; Springer Series in Chemical Physics;* Benninghoven, A., Ed.; Springer-Verlag; Berlin, 1983, Chapter 3.

37)   Beckey, H. D. *J. Mass Spectrom. Ion Physics* **1969**, *2*, 500-503.

38)   Beckey, H. D. *Principles of Field Ionization and Field Desorption Mass Spectrometry; International Series in Analytical Chemistry, Vol. 61;* Belcher, R., Frieser, H., Eds.; Pergamon Press: Oxford, England, 1977.

39)   Schulten, H.-R. *Int. J. Mass Spectrom. Ion Physics* **1979**, *32*, 97-283.

40)   Wada, Y.; Hayashi, A.; Fujita, T.; Matsuo, T.; Katakase, I.; Matsuda, H. *Biochim. Biophys. Acta.* **1981**, *667,* 233-241.

41)   Tanaka, K.; Waki, H.; Ido, Y.; Akita, S.; Yoshida, Y.; Yoshida, T. *Rapid Commun. Mass Spectrom.* **1988**, *2*, 151-153.

42)   Karas, M.; Hillenkamp, F. *Anal. Chem.* **1988**, *60*, 2299-2301.

43)   Beavis, R. C.; Chait, B. T. *Rapid Commun. Mass Spectrom.* **1989**, *3*, 233-237.

44)   Marshall, A. G.; Grosshans, P. B. *Anal. Chem.* **1991**, *63*, 215 A-229 A.

45)   Marshall, A. G.; Roe, D. C. *J. Chem. Phys.* **1980**, *73*, 1581-1590.

46)   Baldeschwieler, J. D.; Randall, E. W. *Chem. Rev.* **1963**, *63*, 81-110.

47)   McIver, R. T., Jr.; Baykut, G.; Hunter, R. L. *Int. J. Mass Spectrom. Ion Processes* **1989**, *89*, 343-358.

48)   McIver, R. T., Jr.; Hunter, R. L.; Baykut, G. *Anal. Chem.* **1989**, *61*, 489-491.

49)   Wang, M.; Marshall, A. G. *Int. J. Mass Spectrom. Ion Processes* **1990**, *100*, 323-346.

50)   Marshall, A. G.; Wang, T. -C. L.; Ricca, T. L. *J. Am. Chem. Soc.* **1985**, *107*, 7893-7897.

51)   Goodman, S.; Hanna, A. *U. S. Patent* 4,945,234, **1990**.

52)   Guan, S. *J. Chem. Phys.* **1989**, *91*, 775-777.

53)   Comisarow, M. B. *J. Chem. Phys.* **1978**, *69*, 4097-4104.

54)   Marshall, A. G. In *Encyclopedia of Nuclear Magnetic Resonance, Vol. 1*; Grant, D. M., Harris, R. K., Eds.; Wiley: London, 1996, pp 486-489.

55)   Villiers, M. A. *C. R. Acad. Sci. Paris* **1891**, *112*, 536-538.

56)   Schardinger, F. *Z. Unters. Nahr. u. Genussm.* **1903**, *6*, 865.

57)   Schardinger, F. *Wien. Klin. Wochenschr.* **1904**, *17*, 207-208.

58)   Schardinger, F. *Zentralbl. Bakteriol. Parasintenk. Abt. 2* **1905**, *14*, 772-781.

59)   Pulley, A. O.; French, D. *Biochem. Biophys. Res. Commun.* **1961**, *5*, 11-15.

60)   Bender, H. *Carbohydr. Res.* **1978**, *65*, 85-97.

61)   Bender, M. L.; Komiyama, M. *Reactivity and Structure Concepts in Organic Chemistry, Vol. 6, Cyclodextrin Chemistry*; Hafner, K., Rees, C. W., Trost, B. M., Lehn, J. M., von Ragué Schleyer, P., Zahradník, R., Eds.; Springer-Verlag: Berlin, 1978.

62)   Hinze, W. L.; Armstrong, D. W. Eds. *Ordered Media in Chemical Separations, ACS Symp. Series*; American Chemical Society: Washington, DC, 1987.

63)   Atwood, J. L.; Davies, J. E. D.; MacNicol, D. D. Eds. *Inclusion Compounds, Vol. 3, Physical Properties and Applications*; Academic Press: London, 1984.

64)   Szejtli, J. *Cyclodextrins and Their Inclusion Complexes*; Akademiai Kiado: Budapest, 1982.

65)   Fendler, J. H.; Fendler, E. J. *Catalysis in Micellar and Macromolecular Systems*; Academic Press: New York, 1975.

66)   Cramer, F. *Einschluβverbindungen*; Springer-Verlag: Berlin, 1954.

67)   Szejtli, J. *Cyclodextrin Technology*; Kluwer Academic Publishers: Dordrecht, 1988.

68)   French, D. In *Advances in Carbohydrate Chemistry, Vol 12;* Wolfrom, M. L., Tipson, R. S., Eds.; Academic Press: New York, 1957, pp 189-260.

69)   Griffiths, D. W.; Bender, M. L. In *Advances in Catalysis, Vol. 23*, Eley, D. D., Pines, H., Weisz, P. B., Eds.; Academic Press: New York, 1973, pp 209-261.

70)   Senti, F. R.; Erlander, S. R. In *Non-Stoichiometric Compounds*; Mandelcorn, L. Ed.; Academic Press: New York, 1964; Chapter 9.

71)   Thome, J. A.; Stewart, L. In *Starch: Chemistry and Technology*; Whistler, R. L., Paschall, E. F., Eds.; Academic Press: New York, 1965, Chapter 9.

72)   Frank, S. G. *J. Pharm. Sci.* **1975**, *64*, 1585-1604.

73)   Saenger, W. In *Environmental Effects on Molecular Structure and Properties*; Pullman, B., Ed.; D. Reidel Publishing Company: Dordrecht-Holland, 1976; pp 265-305.

74)   Bergeron, R. J. *J. Chem. Educ.* **1977**, *54*, 204-207.

75)   Mifune, A.; Shima, A. *J. Synth. Org. Chem. Jpn.* **1977**, *35*, 116-130.

76)   Bender, M. L.; Komiyama, M. In *Bioorganic Chemistry, Vol. 1*; van Tamelen, E. E., Ed.; Academic Press: New York, 1977, pp 19-57.

77)   MacNicol, D. D.; McKendrick, J. J.; Wilson, D. R. *Chem. Soc. Rev. (London)* **1978**, *7*, 65-87.

78)   Breslow, R. *Adv. Chem. Ser.* **1980**, *191*, 1-15.

79)   Saenger, W. *Angew. Chem. Int. Ed. Engl.* **1980**, *19*, 344-362.

80)   Hinze, W. L. *Sep. Purif. Methods* **1981**, *10*, 159-237.

81)   Smolková-Keulemansová, E. *J. Chromatogr.* **1982**, *251*, 17-34.

82)   Szejtli, J. In *Inclusion Compounds, Vol. 3, Physical Properties and Applications*; Atwood J. L., Davies, J. E. D., MacNicol, D. D., Eds.; Academic Press: New York, 1984, Chapter 11.

83) Tabushi, I. In *Inclusion Compounds, Vol. 3, Physical Properties and Applications*; Atwood J. L., Davies, J. E. D., MacNicol, D. D., Eds.: Academic Press: New York, 1984, Chapter 13.

84) Szejtli, J.; Zsadon, B.; Cserhati, T. In *Ordered Media in Chemical Separations, ACS Symp. Series*; Hinze, W. L., Armstrong, D. W., Eds., American Chemical Society: Washington, DC, 1987, Chapter 11.

85) Sundararajan, P. R.; Rao, V. S. R. *Carbohyd. Res.* **1970**, *13*, 351-358.

86) French, D.; Pulley, A. O.; Effenberger, J. A.; Rougvie, M. A.; Abdullah, M. *Arch. Biochem. Biophys.* **1965**, *111*, 153-160.

87) Bakhtiar, R.; Kaifer, A. E. *Rapid Commun. Mass Spectrom.* **1998**, *12*, 111-114.

88) Prokai, L.; Ramanathan, R.; Nawrocki, J.; Eyler, J. *J. Inclusion Phen. Mol. Recogn. Chem.* **1996**, *25*, 117-120.

89) Ramanathan, R.; Prokai, L. *J. Am. Soc. Mass Spectrom.* **1995**, *6*, 866-871.

90) Ramirez, J.; He, F.; Lebrilla, C. B. *J. Am. Chem. Soc.* **1998**, *120*, 7387-7388.

91) Penn, S. G.; He, F.; Green, M. K.; Lebrilla, C. B. *J. Am. Soc. Mass Spectrom.* **1997**, *8*, 244-252.

92) Camilleri, P.; Haskins, N. J.; New, A. P.; Saunders, M. R. *Rapid Commun. Mass Spectrom.* **1993**, *7*, 949-952.

93) Schaschke, N.; Fiori, S.; Weyher, E.; Escrieut, C.; Fourmy, D.; Müller, G.; Moroder, L. *J. Am. Chem. Soc.* **1998**, *120*, 7030-7038.

94) Cescutti, P.; Garozzo, D.; Rizzo, R. *Carbohyd. Res.* **1996**, *290*, 105-115.

95) Mele, A.; Selva, A. *J. Mass Spectrom.* **1995**, *30*, 645-647.

96) Selva, A.; Redenti, E.; Zanol, M.; Ventura, P.; Casetta, B. *Org. Mass Spectrom.* **1993**, *28*, 983-986.

97) Cahill, S.; Rinzler, A. G.; Owens, F. J.; Bulusu, S. *J. Phys. Chem.* **1994**, *98*, 7095-7100.

98) Szejtli, J. *Starch*, **1990**, *42*, 444-447.

99) Pedersen, C. J. *J. Am. Chem. Soc.* **1967**, *89*, 2495-2496.

100) Pedersen, C. J. *J. Am. Chem. Soc.* **1967**, *89*, 7017-7036.

101) Connors, K. A. *Chem. Rev.* **1997**, *97*, 1325-1357.

102) Carr, S. A.; Hemling, M. E.; Bean, M. F.; Roberts, G. D. *Anal Chem.* **1991**, *63*, 2802-2824.

103) Bruce, J. E.; Anderson, G. A.; Udseth, H. R. *Anal. Chem.* **1998**, *70*, 519-525.

104) Weiskopf, A. S.; Vouros, P.; Harvey, D. J. *Anal. Chem.* **1998**, *70*, 4441-4447.

105) Deforce, D. L. D.; Raymackers, J.; Meheus, L. *Anal. Chem.* **1998**, *70*, 3060-3068.

106) Wilson, S. R.; Wu, Y. *J. Am. Chem. Soc.* **1993**, *115*, 10334-10337.

107) Hunt, S. M.; Sheil, M. M.; Belov, M. *Anal. Chem.* **1998**, *70*, 1812-1822.

108) Katta, V.; Chowdhury, S. K.; Chait, B. T. *J. Am. Chem. Soc.* **1990**, *112*, 5348-5349.

109) Yamashita, M.; Fenn, J. B. *J. Phys. Chem.* **1984**, *88*, 4671-4675.

110) Fenn, J. B.; Mann, M.; Meng, C. K.; Wong, S. F.; Whitehouse, C. M. *Science* **1989**, *246*, 64-71.

111) Covey, T. R.; Bonner, R. F.; Shushan, B. I.; Henion, J. *Rapid Commun. Mass Spectrom.* **1988**, *2*, 249-256.

112) Smith, R. D.; Olivares, J. A.; Nguyen, N. T.; Udseth, H. R. *Anal. Chem.* **1988**, *60*, 436-441.

113) Loeb, L. B.; Kip, A. F.; Hudson, G. G.; Bennett, W. H. *Phys. Rev.* **1941**, *60*, 714-722.

114) Pfeifer, R. J.; Hendricks, C. D. *AIAA J.* **1968**, *6*, 496-502.

115) Kebarle, P.; Tang, L. *Anal. Chem.* **1993**, *65*, 972 A-986 A.

116) Taylor, G. I. *Proc. R. Soc. London A* **1964**, *280*, 383-397.

117) Gomez, A.; Tang, K. *Proceedings of the Fifth International Conference on Liquid Atomization and Spray Systems (ICLASS-91)*; Smerjians, H. G., Ed.; NIST: Gaithersburg, MD; Special Publication 813, 1991, pp 771-778.

118) Gomez, A.; Tang, K. *Physics of Fluids* **1994**, *6*, 404-414.

119) *Lord Rayleigh Philos. Mag.* **1882**, *14*, 184.

120) Taflin, D. C.; Ward, T. L.; Davis, E. J. *Langmuir* **1989**, *5*, 376-384.

121) Davis, E. J. *ISA Trans.* **1987**, *26*, 1.

122) Willoughby, R.; Sheehan, E.; Jarrell, A.; Pedder, R.; Marecic, T.; Penn, S. *Proceedings of the 41st American Society for Mass Spectrometry Conference on Mass Spectrometry and Allied Topics*, San Francisco, CA, 1993, p 765.

123) Sheehan, E. W.; Willoughby, R. C. *Proceedings of the 41st American Society for Mass Spectrometry Conference on Mass Spectrometry and Allied Topics*, San Francisco, CA, 1993 p 770.

124) Iribarne, J. V.; Thomson, B. A. *J. Chem. Phys.* **1976**, *64*, 2287.

125) Thomson, B. A.; Iribarne, J. V. *J. Chem. Phys.* **1979**, *71*, 4451-4463.

126) Wachs, T.; Bente, P. F., III; McLafferty, F. W. *Int. J. Mass Spectrom. Ion Phys.* **1972**, *9*, 333-341.

127) Bozorgzadeh, M. H.; Morgan, R. P.; Beynon, J. H. *Analyst* **1978**, *103*, 613-622.

128) Kondrat, R. W.; Cooks, R. G. *Anal. Chem.* **1978**, *50*, 81 A-92 A.

129) Yost, R. A.; Enke, C. G. *J. Am. Chem. Soc.* **1978**, *100*, 2274-2275.

130) Comisarow, M. In *Advances in Mass Spectrometry, Vol. 7B*; Daly, N. R., Ed.; Heyden and Son: London, 1978, pp 1042-1046.

131) Kaplan, F. *J. Am. Chem. Soc.* **1968**, *90*, 4483-4485.

132) van der Hart, W. J.; van Sprang, H. A. *J. Am. Chem. Soc.* **1977**, *99*, 32-35.

133) Henis, J. M. S. *J. Am. Chem. Soc.* **1968**, *90*, 844-851.

134) Bensimon, M.; Houriet, R. *Int. J. Mass Spectrom. Ion Processes* **1986**, *72*, 93-98.

135) Cody, R. B.; Burnier, R. C.; Freiser, B. S. *Anal. Chem.* **1982**, *54*, 96-101.

136) Dunbar, R. C. Case Western Reserve University, Unpublished Results.

137) Freiser, B. S. *Talanta* **1985**, *32*, 697-708.

138) McLafferty, F. W.; Amster, I. J. *Int. J. Mass Spectrom. Ion Processes* **1986**, *72*, 85-91.

139) Gord, J. R.; Freiser, B. S. *Anal. Chim. Acta* **1989**, *225*, 11-24.

140) Todd, P. J.; McLafferty, F. W. In *Tandem Mass Spectrometry*; McLafferty, F. W., Ed.; Wiley: New York, 1983, pp 149-174.

141) Levsen, K. *Fundamental Aspects of Organic Mass Spectrometry*; Verlag Chemie, Weinheim: New York, 1978.

142) Brenton, A. G.; Morgan R. P.; Beynon, J. H. *Ann. Rev. Phys. Chem.* **1979**, *30*, 51-78.

143) Rosenstock, H. M.; Wallenstein, M. B.; Wahrhaftig, A. L.; Eyring, H. *Proc. Natl. Acad. Sci. U.S.A.* **1952**, *38*, 667-678.

144) Marcus, R. A.; Rice, O. K. *J. Phys. Colloid Chem.* **1951**, *55*, 894-908.

145) Baer, T. In *Mass Spectrometry, Vol. 6*; The Royal Society of Chemistry, Burlington House: London, 1981, Chapter 1.

146) Schwartz, R. N.; Slawsky, Z. I.; Herzfeld, K. F. *J. Chem. Phys.* **1952**, *20*, 1591-1599.

147) Douglas, D. J. *J. Phys. Chem.* **1982**, *86*, 185-191.

148) Boyd, R. K.; Kingston, E. E.; Brenton, A. G.; Beynon, J. H. *Proc. Royal Soc. London A*, **1984**, *392*, 89-106.

149) Nystrom, J. A.; Bursey, M. M.; Hass, J. R. *Int. J. Mass Spectrom. Ion Processes* **1983/1984**, *55*, 263-274.

150) Bursey, M. M.; Nystrom, J. A.; Hass, J. R. *Anal. Chim. Acta* **1984**, *159*, 265-274.

151) Bursey, M. M.; Nystrom, J. A.; Hass, J. R. *Anal. Chim. Acta* **1984**, *159*, 275-282.

152) Alexander, A. J.; Thibault, P. *Rapid Commun. Mass Spectrom.* **1988**, *2*, 224-228.

153) Nawrocki, J. Ph. D. Dissertation, University of Florida, **1997**.

154) Caravatti, P. *U. S. Patent* 4,924,089, **1990**.

155) Harvey, R. G., Ed. *Polycyclic Hydrocarbons and Carcinogenesis*; American Chemical Society: Washington, DC, 1985.

156) Léger, A.; d'Hendecourt, L. B. *Astron. Astrophys.* **1985**, *146*, 81-85.

157) Omont, A. *Astron. Astrophys.* **1986**, *164*, 159-178.

158) Allamandola, L. J.; Tielens, A. G. G. M.; Barker, J. R. *Astrophys. J. Suppl. Ser.* **1989**, *71*, 733-775.

159) Turner, B. E. *Space Sci. Rev.* **1989**, *51*, 235-337.

160) Puget, J. L.; Léger, A. *Annu. Rev. Astron. Astrophys.* **1989**, *27*, 161-198.

161) Allamandola, L. J. *Top. Curr. Chem.* **1990**, *153*, 1-25.

162) Allamandola, L. J. *Chemistry and Spectroscopy of Interstellar Molecules*; Tokyo University Press: Tokyo, 1992.

163) Platt, J. R. *Astrophys. J.* **1956**, *123*, 486-490.

164) Gillet, F. C.; Forrest, W. J.; Merrill, K. M. *Astrophys. J.* **1973**, *183*, 87-93.

165) Aitken, D. K. In *Infrared Astronomy*; Wynn-Williams, C. G., Cruikshank, D. P., Eds.; Reidel: Dortrecht, 1981; p 207-221.

166) Willner, S. P. In *Galactic and Extragalactic Infrared Spectroscopy*; Kessler, M. F., Phillips, J. P., Eds.; D. Reidel: Dortrecht, 1984; p 37-57.

167) Sellgren, K. *Astrophys. J.* **1984**, *277*, 623-633.

168) Beichman, C. A.; Keene, J.; Phillips, T. G.; Huggins, P. J.; Wootten, H. A. *Astrophys. J.* **1983**, *273*, 633-638.

169) Phillips, M. M.; Aitken, D. K.; Roche, P. F. *Mon. Not. R. Astr. Soc.* **1984**, *207*, 25-33.

170) Low, F. J.; Beintema, D. A.; Gautier, T. N.; Gillett, F. C.; Beichman, C. A.; Neugebauer, G.; Young, E.; Auman, H. H.; Boggess, N.; Emerson, J. P.; Habing, H. J.; Hauser, M. G.; Houck, J. R.; Rowan-Robinson, M.; Soifer, B. T.; Walker, R. G.; Wesselius, P. R. *Astrophys. J. (Lett.)* **1984**, *278*, L19-L22.

171) Allamandola, L. J.; Norman, C. A. *Astron. Astrophys.* **1978**, *66*, 129-135.

172) Allamandola, L. J.; Greenberg, J. M.; Norman, C. A. *Astron. Astrophys.* **1979**, *77*, 66-74.

173) Duley, W. W.; Williams, D. A. *Mon. Not. R. Astr. Soc.* **1981**, *196*, 269-274.

174) Allamandola, L. J. In *Galactic and Extragalactic Infrared Spectroscopy*, Kessler, M. F., Phillips, J. P., Eds.; D. Reidel: Dortrecht, 1984; pp 5-35.

175) Léger, A.; Puget, J. L. *Astron. Astrophys.* **1984**, *137*, L5-L8.

176) Allamandola, L. J.; Tielens, A. G. G. M.; Barker, J. R. *Astrophys. J. (Lett.)* **1985**, *290*, L25-L28.

177) van der Zwet, G. P.; Allamandola, L. J. *Astron. Astrophys.* **1985**, *146*, 76-80.

178) Crawford, M. K.; Tielens, A. G. G. M.; Allamandola, L. J. *Astrophys. J.* **1985**, *293*, L45-L48.

179) Salama, F.; Allamandola, L. J. *J. Chem. Phys.* **1991**, *94*, 6964-6977.

180) Roche, P. F.; Aitken, D. K.; Smith, C. H. *Mon. Not. R. Astr. Soc.* **1989**, *236*, 485-494.

181) Duley, W. W.; Jones, A. P. *Astrophys. J.* **1990**, *351*, L49-L52.

182) Heger, M. L. *Lick Obs. Bull.* **1922**, *10*, 146.

183) Krelowski, J.; Sneden, C. In *The Diffuse Interstellar Bands, Vol. 202;* Tielens, A. G. G. M., Snow, T. P., Eds.; Kluwer Academic Publishers: Dordrecht, 1995, pp 13-24.

184) Johnson, F. M. *Spectroscopic Studies of Interstellar Grains*; NASA CR, 1970.

185) Herbig, G. H. *Astrophys. J.* **1975**, *196*, 129-160.

186) Jenniskens, P.; Desert, F. X. *Astron. Astrophys. Suppl. Ser.* **1994**, *106*, 39-78.

187)   Krelowski, J.; Walker, G. A. H. *Astrophys. J.* **1987**, *312*, 860-867.

188)   Foing, B. H.; Ehrenfreund, P. *Nature* **1994**, *369*, 296-298.

189)   Shida, T.; Iwata, S. *J. Am. Chem. Soc.* **1973**, *95*, 3473-3483.

190)   Pankasem, S.; Thomas, J. K. *J. Phys. Chem.* **1991**, *95*, 7385-7393.

191)   Kira, A.; Imamura, M.; Shida, T. *J. Phys. Chem.* **1976**, *80*, 1445-1448.

192)   Karger, W.; Fordham, R. J.; Dubois, J. J.; Glaude, P. G. J. M.; Ligthart, J. A. M. *Spectral Atlas of Polycyclic Aromatic Compounds*; Commission of European Communities, Ed.; Reidel: Dordecht, 1983, pp 92-95.

193)   Clar, E.; Schmidt, W. *Tetrahedron* **1976**, *32*, 2563-2566.

194)   Bondybey, V. E.; Miller, T. A. In *Molecular Ions: Spectroscopy, Structure, and Chemistry*; Miller, T. A., Bondybey, V. E., Eds.; North-Holland: New York, 1983, pp 125-173.

195)   Boissel, P.; Lefèvre, G.; Thiébot, Ph. In *Proceedings of the Conference on Physical Chemistry of Molecules and Grains in Space, Mt Ste Odile, France*; American Institute of Physics: New York, 1993, pp 667-674.

196)   Ekern, S. P.; Marshall, A. G.; Szczepanski, J.; Vala, M. *Astrophys. J.* **1997**, *488*, L39-L41.

197)   Wang, X.; Becker, H.; Hopkinson, A. C.; March, R. E.; Scott, L. T.; Böhme, D. K. *Int. J. Mass Spectrom. Ion Processes* **1997**, *161*, 69-76.

198)   Ekern, S. P.; Marshall, A. G.; Szczepanski, J.; Vala, M. *J. Phys. Chem. A* **1998**, *102*, 3498-3504.

199)   Harvey, R. G. *Polycyclic Aromatic Hydrocarbons*; Wiley-VCH: New York, 1997.

200)   Vala, M.; Szczepanski, J. University of Florida, Unpublished results.

201)   Kuo, C.-H.; Tsau, M.-H.; Weng, D. T.-C.; Lee, G. H.; Peng, S.-M.; Luh, T.-Y. *J. Org. Chem.* **1995**, *60*, 7380-7381.

202)   Pogodin, S.; Biedermann, P. U.; Agranat, I. *J. Org. Chem.* **1997**, *62*, 2285-2287.

203) Lee, J.-S.; Nyburg, S. C. *Acta Cryst.* **1985**, *C41*, 560-567.

204) Livingston, R.; Wei, K. S. *J. Phys. Chem.* **1967**, *71*, 541-547.

205) Bowen, E. J.; Marsh, J. D. F. *J. Chem. Soc.* **1947**, *Part I*, 109-110.

206) Dunitz, J. D.; Weissman, L. *Acta Cryst.* **1949**, *2*, 62-63.

207) Welberry, T. R. *Acta Cryst.* **1971**, *B27*, 360-365.

208) Dziewoński, K.; Rapalski, G. *Ber. Deutsch. Chem. Jes.* **1912**, *45*, 2491-2493.

209) Magnus, P.; Morris, J. C.; Lynch, V. *Synthesis* **1997**, *No. 5*, 506-508.

BIOGRAPHICAL SKETCH

David Kage was born on June 15, 1969 in Galesburg, Illinois. He grew up in East Galesburg, where he attended grade school. He then attended middle and high school in Knoxville, Illinois, graduating in 1987. High school was where he became interested in science thanks to Mr. Ron Zarn, his teacher for algebra, geometry, trigonometry, calculus, physics I and II, and of course chemistry I and II.

During the next six years, he attended Illinois State University in Normal, Illinois, where he received his B.S. degree in chemistry in May of 1991 and his M.S. degree in chemistry in August of 1993. His thesis, "The Effects Of Extra Neutrons In The Carbon And Hydrogen Framework Upon The Thermodynamics Of Intermolecular Electron Transfer," involved isotope enrichments utilizing the differences in solution electron affinities between aromatic hydrocarbons and their isotopically substituted analogues.

He immediately began his studies at the University of Florida in the fall of 1993. While attending the University of Florida, he decided to try a different area of experimental physical chemistry, so he joined the research laboratory of Dr. John Eyler. His current research interests are photodissociation studies of gas-phase polycyclic aromatic hydrocarbons of interstellar importance utilizing Fourier transform ion cyclotron resonance mass spectrometry.

I certify that I have read this study and that in my opinion it conforms to acceptable standards of scholarly presentation and is fully adequate, in scope and quality, as a dissertation for the degree of Doctor of Philosophy.

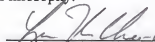John R. Eyler, Chairman
Professor of Chemistry

I certify that I have read this study and that in my opinion it conforms to acceptable standards of scholarly presentation and is fully adequate, in scope and quality, as a dissertation for the degree of Doctor of Philosophy.

William Weltner
Professor of Chemistry

I certify that I have read this study and that in my opinion it conforms to acceptable standards of scholarly presentation and is fully adequate, in scope and quality, as a dissertation for the degree of Doctor of Philosophy.

Robert J. Hanrahan
Professor of Chemistry

I certify that I have read this study and that in my opinion it conforms to acceptable standards of scholarly presentation and is fully adequate, in scope and quality, as a dissertation for the degree of Doctor of Philosophy.

Lisa McElwee-White
Professor of Chemistry

I certify that I have read this study and that in my opinion it conforms to acceptable standards of scholarly presentation and is fully adequate, in scope and quality, as a dissertation for the degree of Doctor of Philosophy.

Laszlo Prokai
Associate Professor of Pharmaceutics

This dissertation was submitted to the Graduate Faculty of the Department of Chemistry in the College of Liberal Arts and Sciences and to the Graduate School and was accepted as partial fulfillment for the degree of Doctor of Philosophy.

December, 1999

Dean, Graduate School

LD
178.
199<u>9</u>
KII